FCTUC **FACULDADE DE CIÊNCIAS E TECNOLOGIA**
UNIVERSIDADE DE COIMBRA

DEPARTAMENTO DE
ENGENHARIA MECÂNICA

Surface Modification of Structural Steels by Friction Stir Processing

Dissertação apresentada para a obtenção do grau de Mestre em Engenharia Mecânica na Especialidade de Produção e Projecto

Autora

Maria Inês Martins dos Santos Costa

Orientadora

Professora Doutora Dulce Maria Esteves Rodrigues

Júri

Presidente	Professor Doutor **Albano A.C. Rodrigues de Carvalho** **Professor Catedrático da Universidade de Coimbra**
Vogais	Professora Doutora **Dulce Maria Esteves Rodrigues** **Professora Auxiliar da Universidade de Coimbra**
	Professor Doutor **Rui António Duarte Simões** **Professor Auxiliar da Universidade de Coimbra**
	Mestre **Carlos Miguel Almeida Leitão** **Investigador do CEMUC**

Colaboração Institucional

ISISE

AIMEN

Coimbra, Setembro, 2013

FCTUC **FACULDADE DE CIÊNCIAS**
E TECNOLOGIA
UNIVERSIDADE DE COIMBRA

DEPARTAMENTO DE
ENGENHARIA MECÂNICA

Surface Modification of Structural Steels by Friction Stir Processing

Author
Maria Inês Martins dos Santos Costa
Superviser
PhD Professor Dulce Maria Esteves Rodrigues
Evaluation Panel

Chair-man   PhD Professor **Albano A.C. Rodrigues de Carvalho**
           Full Professor University of Coimbra

Committee   PhD Professor **Dulce Maria Esteves Rodrigues**
           Assistant Professor University of Coimbra

           PhD Professor **Rui António Duarte Simões**
           Assistant Professor da Universidade de Coimbra

           Master **Carlos Miguel Almeida Leitão**
           CEMUC Investigator

Institutional Collaboration

ISISE

AIMEN

Coimbra, September, 2013

"Cada adversidade, cada falhanço e cada desgosto trazem consigo a semente de um benefício equivalente ou ainda maior."

Napolean Hill

Aos meus pais e avós.

Agradecimentos

No culminar de mais uma etapa da minha vida existem algumas pessoas às quais não posso deixar de agradecer, todos aqueles que contribuíram, directa ou indirectamente, para o meu sucesso, quer na realização da tese, quer ao longo da minha vida académica e pessoal.

À minha orientadora, a Professora Doutora Dulce Rodrigues pela dedicação, paciência, encorajamento, e também pelos "puxões de orelhas" nos momentos certos seguidos dos ensinamentos que tanto me fizeram evoluir.

Ao Aimen, na pessoa do Engenheiro David Gesto, pela disponibilidade demonstrada para a realização do processamento das superfícies.

Ao Professor Doutor Amílcar Ramalho, agradeço pela disponibilidade demonstrada para a partilha de conhecimentos técnicos e científicos.

Ao Mestre Carlos Leitão, um obrigado muito especial, pelos seus ensinamentos, por toda a paciência, disponibilidade e pela boa disposição que o caracterizam e que muito me ajudaram nos momentos de maior dificuldade.

Aos elementos do Grupo de Tecnologia, um sincero obrigado pela forma como fui acolhida, pelas sugestões e amizade.

Aos colegas de laboratório, como não poderia deixar de ser, quero agradecer os bons momentos passados, a entreajuda, companheirismo e a inegável amizade, que contribuíram para a minha motivação até nas alturas de maior desgaste.

Aos meus pais, quero prestar um reconhecimento especial pelo estímulo e apoio incondicional com que sempre pude contar; pelas palavras sensatas que muito me ajudaram e por nunca deixarem de acreditar e investir em mim e nas minhas capacidades, mesmo nos momentos mais difíceis. Também não posso deixar de agradecer por me transmitirem os seus valores, a noção de humildade, carácter e ética, pelos seus bons exemplos pessoais e profissionais.

Aos meus avós com quem sempre pude contar no bem e no mal, que me ajudaram a crescer com muito amor e carinho, desde a menina activa que fugia de casa para ir brincar na rua até à idade adulta, e gostam até deste meu "mau-feitio".

Aos meus familiares, agradeço o constante incentivo recebido ao longo da minha vida.

Ao Paulo Cristóvão quero agradecer os conselhos e o incentivo, mas principalmente por saber sempre o que dizer nos momentos certos, e ser a única pessoa no mundo capaz de meter o meu computador, muito temperamental, a funcionar devidamente.

Ao João Mendes quero agradecer pelo companheirismo dos últimos 5 anos.

Aos meus amigos, a segunda família, quero agradecer a força a compreensão e as memórias, devo-vos um pedido de desculpa por ter estado um pouco mais ausente.

A todos,

O meu mais sincero obrigado.

Resumo

Nesta tese, são analisadas a microestrutura bem como as propriedades mecânicas e tribológicas das superfícies de aços estruturais processadas/texturizadas por um processo baseado no Friction Stir Welding (FSW), denominado por Friction Stir Processing (FSP).

As superfícies dos aços estruturais, S275 e S690, foram processadas por duas ferramentas de WC-Co, sem pino e de bases de diferentes diâmetros, variando em cada processamento, as suas velocidades de rotação e avanço. Espera-se que o comportamento tribológico das superfícies processadas seja influenciado pela sua morfologia, a qual revelou ser muito regular para ambos os materiais, quando processados pela ferramenta de menor diâmetro. Observou-se que a texturização da superfície variou com a relação das velocidades de rotação e de avanço da ferramenta, para ambos os substratos.

A análise microestrutural das superfícies processadas revelou um importante refinamento de grão na zona processada, independentemente do material e das suas condições de processamento. A resistência mecânica das zonas processadas foi avaliada através de testes de dureza, sendo que se verificou que também esta aumentou drasticamente relativamente à dureza dos substratos. No caso do aço S275 não ocorreram variações da dureza para amostras processadas com a variação da velocidade de avanço da ferramenta, desde que se mantenha constante a sua velocidade de rotação. Contudo, verificou-se que, para a mesma velocidade de avanço da ferramenta, o aumento da velocidade de rotação, ou seja, o aumento do calor induzido pela ferramenta no substrato, aumenta a dureza obtida. No caso do aço S690, a dureza obtida não se alterou com a variação das velocidades de avanço e rotação da ferramenta. Quer a elevada temperabilidade dos aços, quer o seu refinamento de grão provaram ser determinantes no aumento da dureza das superfícies processadas. Finalmente, os testes de fricção realizados em amostras de S275, revelaram um aumento de 100% do coeficiente de fricção estática bem como na rigidez da ligação amostra/contra-corpo das amostras processadas relativamente às não processadas.

Palavras-chave: Aços estruturais, Friction Stir Processing, Texturização superficial, Dureza, Comportamento à fricção.

[This page intentionally left blank]

[This page intentionally left blank]

Abstract

The microstructural, mechanical and tribological properties of processed/textured structural steel surfaces, produced using a Friction Stir Welding (FSW) related procedure, called Friction Stir Processing (FSP), are analysed in this thesis.

The surface of S275 and S690 structural steels samples was processed using two WC-Co pinless tools, with different diameters, and varying tool rotation and traverse speeds. The morphology of the surfaces, which is expected to have an important influence on its tribological behaviour, revealed to be very regular, for both materials, when processing with the lower diameter tool. Surface texture was also observed to evolve, according to the tool rotation to tool traverse speed ratio, for both substrates.

Microstructural analysis of the processed surfaces revealed an important grain refinement in the stirred zone, independently of the material processed and of the processing conditions. The mechanical strength of the refined structures, evaluated trough hardness tests, was also found to drastically increase, relative to both substrates initial hardness. For the S275 steel, no hardness evolution was found when varying the tool traverse speed at a constant tool rotation speed. On the other hand, an important increase in surface hardness was found when increasing the tool rotation speed, i.e. when increasing the heat input during processing. For the S690 steel no important variation was found when varying, nor the tool rotation speed, nor the tool traverse speed. Both the grain refinement and the high hardenability of both steels, were found to be determinant for the hardness increase of the processed surfaces. Finally, the friction tests performed on S275 samples, revealed a 100% enhancement in the static friction coefficient, as well as in the assembly stiffness, of the processed surface relative to the unprocessed one.

Keywords Structural Steels, Friction Stir Processing, Surface Texturing, Hardness, Friction Behaviour

[This page intentionally left blank]

[This page intentionally left blank]

Contents

[This page intentionally left blank]

FIGURES INDEX

TABLES INDEX

[This page intentionally left blank]

[This page intentionally left blank]

SYMBOLS AND ABBREVIATIONS

Symbols

a – Constant (Torque Equation)

b – Constant (Torque Equation)

C_{eq} – Carbon Equivalent

d_{HV} – Diagonal (Hardness Vickers Equation)

d – Grain size (Hall-Petch Equation)

F_T – Tangential Force

F_N – Normal Force

F_z – Plunging Force

H – Hardness

H_0 – Constant (Hall-Petch equation)

HV – Hardness Vickers

K – Connection Stiffness

k_h – Constant (Hall-Petch equation)

k_s – Slip Coefficient

m – Slip Plates

n – Bolts in The Connection

P – Test Load

P_{slip} – Slip Load

T_i – Clamping Force

v – Tool Traverse Speed

$\propto$ – Tool Tilt Angle

μ_s – Static Friction Coefficient

ω – Tool Rotation Speed

τ – Torque

Abbreviations

AIMEN – Associación de Investigacíon Metalúrgica del Noroeste

AISI – American Iron and Steel Institute

ASM – American Society for Metals

ASTM – American Society for Testing and Materials

BM – Base Material

CEMUC – Centro de Engenharia Mecânica da Universidade de Coimbra

DEM – Departamento de Engenharia Mecânica

EBSD – Electron Backscatter Diffraction

FCTUC – Faculdade de Ciências e Tecnologia da Universidade de Coimbra

FSP – Friction Stir Processing

FSW – Friction Stir Welding

HAZ – Heat Affected Zone

IF – Interstitial Free

ISISE – Instituto para a Sustentabilidade e Inovação em Estruturas de Engenharia

PM – Powder Metallurgy

PCBN – Polycrystalline cubic boron nitride

TMAZ – Thermo Mechanically Affected Zone

TWI – The Welding Institute

UFG – Ultra Fine Grained

1. INTRODUCTION

In the last two decades, welding research in domains requiring enhanced technical solutions conducted to the development of new manufacturing processes, such as the Friction Stir Welding (FSW) and Friction Stir Processing (FSP) techniques, both based on the same solid state processing technology. A non-consumable rotating tool is plunged into the interface between the materials to be joined, in the case of FSW, or onto the surface of the materials to be transformed, in the case of FSP, producing localized heating by interfacial friction. Heating raises locally the temperature of the materials, which are softened and subjected to intense plastic deformation, under the stirring action of the rotating tool being displaced along predefined work paths. The thermomechanical phenomena occurring inside the material volume being stirred enables severe material mixing, and deep metallurgical and structural reactions, which completely transform the properties of the materials being processed. This is the reason why, despite being developed for solid state welding of light metals, this solid state technology rapidly became a promising technique to be used in materials processing, being already applied in the production of superplastic and composite materials, in the mechanical enhancement of cast alloys or in the development of wear resistant surfaces.

However, in spite of the broad range of works published on surface processing, the potential of the FSP techniques for surface texturing, featuring the production of high friction surfaces to be applied in slip resistant connections, is still unexplored, and for this reason was established as the subject of current investigation. More precisely, the objective of this work was the production of texturized surfaces, by FSP of structural steels traditionally used in metallic construction. The substrate materials used were an hot rolled carbon-manganese steel, the S275 steel, and a quenched and tempered steel, the S690 steel. Due to the very hard nature of both substrates to be processed/textured, WC-Co pinless tools were used. The use of this very simple geometry envisaged simultaneously to assist in tools production, as well as to diminish the tool wear during service life. In order to promote different surface finishing conditions, varying processing parameters were used,

i.e. two different tool shoulder dimensions were tested for a large range of tool rotation and advancing speeds.

The surfaces morphology, microstructure and mechanical properties were evaluated by means of visual inspection and standard metallographic and hardness testing procedures. Friction tests, enabling to evaluate the stiffness and static friction coefficients of the textured surfaces, were performed by using an original equipment developed at CEMUC. The coulomb friction linear model, which is the more widely used model to characterize the effect of friction in sliding contacts, was used to determine the static friction coefficient.

Having in mind the objectives of current work, a better insight on the FSP technique and applications, as well as on the improvements already obtained in applying this technology in the processing of several ferrous and non-ferrous materials, will be provided in the thesis State Of Art. In this chapter, the most traditional surface treatments used to improve the oxidation resistance, texturing and slip resistance of structural steels are also reviewed. The next chapters describe sequentially the experimental procedures, the experimental results and the main conclusions resulting from the analysis performed.

2. STATE OF ART

2.1. Friction Stir Processing

2.1.1.　Process Development

In the past decades, when machines and processes environmental and energetic efficiency became one of the most important industrial concerns, the Friction Stir Processing (FSP) technology was developed and commercialised as being a sustainable solid state processing technique. This material processing technology, developed by Mishra et al (2000), at The Welding Institute (TWI), firstly aimed the production of superplastic aluminium alloys. Superplasticity, which can be defined as the ability of metallic alloys to withstand more than 200% uniform tensile elongation, is important for producing complex-shapes. Martin and Evans (2000), for example, discuss the advantages of applying superplastic materials in aircraft components, arguing that this solution enables decreasing the weight of the structures, as well as its cost by increasing productivity.

In order to develop the FSP technique, Mishra et al. (2000) adapted a well-known solid state welding technology, the Friction Stir Welding (FSW) technology, to be used in solid state processing. Since its development by Mishra et al. (2000), the contributions to improve the FSP technology don't stop to increase. Beyond the production of superplastic materials, this technology is also being tested for the homogenization of powder metallurgy (PM) aluminium alloys, metal matrix composites and cast aluminium alloys(Berbon et al. 2001; Spowart et al. 2003; Ma et al. 2003), for the fabrication of surface composites (Mishra et al. 2002) or simply for surface enhancement by dynamic recrystallization. Actually, the FSP technique is emerging as a very effective solid-state processing technique that can provide localized modification and control of microstructures in the near-surface layers of processed metallic components. This last application was the main object of current work and, for this reason, is the main subject of the thesis bibliographic revision.

2.1.2. Process Description

As the FSW technology, the FSP technique uses localized heat, produced by a non-consumable rotating tool that also promotes intense plastic deformation of the stirred material. In Figure 2.1 is provided a sketch of the process, showing the FSP tool as well as the main processing parameters with influence in final processing results. As shown in the figure, a specially designed rotating tool is plunged into the material to be processed and then traversed along a linear trajectory. The heat necessary to perform the processing is achieved by the friction between the tool and the workpiece and by the plastic deformation of the material.
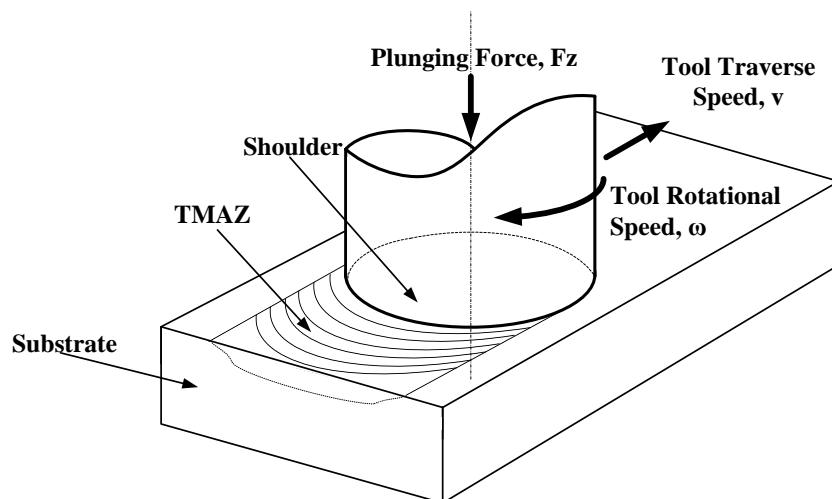
Figure 2.1. Friction stir processing scheme

The most conventional FSP/FSW tools are constituted by a large cylindrical shoulder, as is shown in Figure 2.1 and a concentric pin with smaller diameter. The large shoulder is the main responsible for heat generation during the process, as well as by the stirring of the material at the surface of components being processed. The pin, which protrudes from the shoulder, promotes the vertical flow of the stirred material, enabling to perform through thickness processing. The depth of the processed zone can be adjusted, between several hundred micrometers and tens of millimetres, by changing the length of

the pin. Achieving an optionally adjusted processed depth is considered one of the main advantages of FSP, since this is feature very difficult to be obtained by using other metalworking techniques. The thermomechanical phenomena occurring inside the material volume being stirred by the FSP tool enables deep metallurgical and structural reactions, which completely transform the properties of the materials being processed. This is the reason why, despite being developed for solid state welding of light metals, this solid state processing technology rapidly became a promising processing technique for producing functional graded materials, exhibiting controlled variation of structural and/or chemical features.

In Figure 2.1, the stirred material transformed during processing is identified as TMAZ, which stand to Thermo Mechanically Affected Zone. Besides the TMAZ, it is easy to find in literature a great variety of works describing the various microstructural zones which can be identified in any processed material. The majority of these works distinguishes three main zones: the unaffected Base Material (BM), which in this work will be labelled substrate, the Heat Affected Zone (HAZ) and the Thermo Mechanically Affected Zone.

Meanwhile the microstructure in the HAZ is only influenced by the heat generated during the process, the microstructure of the TMAZ is affected by both the heat and plastic deformation, being characterized by a dynamically recrystalized microstructure. Several investigations demonstrated that grain refinement in the TMAZ of aluminium alloys, carbon steel and brass could be achieved in FSP, provided that the peak temperature during processing is not excessively high. The reason for this is the intense plastic deformation taking place inside the TMAZ, which according to Çam (2011) is the crucial factor in determining the grain size of the recrystallised grains. Increasing degrees of deformation promote dynamic recrystallization and grain refinement takes place, according to the general principles of recrystallization.

As shown in Figure 2.1, the main FSP parameters are the tool rotation speed (ω), the tool traverse speed (v) and the plunging force (F_z), when processing is performed in load control, or the tool penetration, when processing is performed in position control. The first implies the selection of an optimal plunging force, which is maintained constant during processing, and the second implies defining a position of the tool, relatively to the workpiece surface, and the subsequent penetration into the workpiece, which should be

maintained during processing. The microstructure and mechanical properties of the processed zone can be accurately controlled by optimizing the tool design, FSP parameters, and in some specific situations, by promoting active cooling/heating of the processed surfaces.

The traverse and rotational speeds, as well as its relationship, are the main parameters in controlling the thermal cycles during the process, and consequently, in determining the size of the recrystallised grains after processing. The choice of these parameters require a delicate equilibrium since excessive rotational speeds and/or slow traverse speeds promote peak temperatures and slow cooling rates which induce grain coarsening after dynamic recrystallization. Actually, based on the ω/v relationship the processing conditions can be classified as hot or cold. Hot when high rotation and small traverse speeds are used, corresponding to an high ω/v ratio, and cold when small rotation and high traverse speeds are used, corresponding to a low ω/v ratio. Simultaneously, the use of high traverse speeds, despite providing high heating/cooling rates and being advantageous in terms of productivity, may disturb the material flow during surface processing, increasing the probability of flash formation, which has deleterious consequences in processed surfaces quality. The tool penetration and the plunging force are also extremely important in heat generation and in minimizing defects as flash formation.

In addition to the parameters shown in Figure 2.1, there are other parameters with importance in processing conditions, as the tool tilt angle, which is the angle between the tool axis and the normal to the surface being processed. For some tool geometries this angle is absolutely necessary to ensure that the material flow moves from the front to the rear of the tool, without being expelled from under it.

2.1.3.   Surface Enhancement by FSP

For many applications, the useful life of components often depends on their surface properties such as the wear resistance. Particularly, light alloys, such as aluminium, magnesium and titanium alloys, which are used extensively in aerospace and automotive industries due to its low density and high strength to weight ratio, display poor resistance to wear and erosion, which constitutes a serious problem concerning its prolonged use.

Important surface improvements are usually obtained by surface coating (Pan et al. 1998; Yoon et al. 2004; Oliveira et al. 2006). However, despite applying thin hard films, such as oxide, nitride, and carbide films, is shown to be effective in raising the service life of many mechanical parts, getting acceptable coating composition and/or excellent adhesion on tool steel substrates, still needs to be worked. An alternative method for surface modification consists in producing desirable microstructures by laser surface hardening (Babu et al. 2011), this technique in spite of providing higher surface hardness, relative to the substrate, results in cellular/dendritic surfaces, which often requires post-heat-treatments in order to improve surface properties. Actually, it is well known that refining the microstructure, resulting from laser remelting, is the unique way of simultaneously enhancing the hardness and toughness properties of the surfaces. Another important limiting factor in using the mentioned surface improvement techniques is that, all of them, require using expensive equipments, such as sputtering systems, lasers or electron beams. Due to the above mentioned difficulties/limitations of traditional surface engineering techniques, solid state processing techniques, such as FSP, become an attractive alternative approach in surface enhancement, by grain refinement, for many kinds of alloys.

Enhancement of local substrate properties by FSP was already performed by several authors in pure aluminium (Yadav and Bauri, 2012); aluminium alloys (Kwon et al. 2003; Santella et al. 2005; Su et al. 2005; Giles et al. 2008); magnesium alloys (Feng and Ma, 2007; Xing-Hao and Bau-Lin, 2008; Albakri et al. 2013); NiAL bronze (Oh-Ishi and McNelley, 2004); titanium alloys (Atapour et al. 2010); copper (Galvão et al. 2012); and steels (Aldajab et al. 2009; Chen and Nakata, 2009; Chabok and Dehghani, 2010; Dehghani and Chabok, 2011; Mehranfar and Dehghani, 2011; Grewal et al. 2013). In all these studies important grain refinement, microstructural homogenization and improved mechanical properties were registered for the processed materials. Some of these works even report the formation of ultrafine grained microstructures (UFG) with relatively uniform microstructure (Su et al. 2005; Xing-Hao and Bau-Lin, 2008; Chabok and Dehghani, 2010; Dehghani and Chabok, 2011).

Analysing the works in literature it is possible to conclude that important improvements in mechanical strength were obtained for several aluminium alloys. Yadav and Bauri (2012), which performed FSP of 12 mm tick plates of pure aluminium, reported

an important grain refinement after processing. The average grain size was reduced in a single processing pass from 84 μm, in the unprocessed material, to an average grain size of 3 μm. This grain refinement improved the substrate hardness and ultimate tensile strength from 29 to 39 $HV_{0,3}$ and from 72 to 90 MPa, respectively. In the same way, Kwon et al. (2003), performed FSP of 1050 aluminium alloy, at varied rotation speeds. These authors concluded that the grain size in the stir zone decreases when decreasing the rotation speed of the tool, from 3 to 4 μm, at 1840 rpm, to 0.5 μm, at 560 rpm. Both the tensile stress and the hardness of the 1840 rpm samples were lower than that of 560 rpm samples. The authors also concluded that the processed materials hardness depended not only on grain size but also on the dislocation density inside of it. On the other hand, Santella et al. (2005), performed FSP of the A356 and A319 alloys, obtaining important improvements in yield stress, ductility and fatigue resistance, for both cast aluminium alloys, by the homogenization by solid state processing of the distribution of second-phase particles and the reduction of cast porosity. Oh-Ishi and McNelley (2004), obtained similar results when processing NiAl bronze.

Most of the studies performed to date, regarding surface enhancement by FSP, envisaged very specific applications. Galvão et al. (2012), were the first to test a broad range of processing conditions. These authors performed processing of copper-DHP, using different tool geometries and processing parameters. They found that the tool geometry, which has a close relation with the plastic deformation and dynamic recrystallization kinetics inside the stirred volume, the processing parameters and the heat exchange conditions, which determine the extent of dynamic recrystallization and annealing, are determinant in processed materials microstructure and mechanical properties.

Regarding the surface processing of ferrous materials, the number and variety of works in literature is much lower than that regarding processing of non-ferrous materials. The range of steels processed by this technique is very small, including surface processing of tool steels (Chen and Nakata, 2009), high carbon steels (Aldajah et al. 2009), interstitial free (IF) steels (Chabok and Dehghani, 2010), austenitic-steels (Mehranfar and Dehghani, 2011) and structural steels (Grewal et al. 2013).

Chen and Nakata (2009), performed processing of the SKD61 tool steel using a polycrystalline cubic boron nitride (PCBN) tool. The authors evaluated the microstructure, tensile properties and wear characteristic of the processed surface material. They reported

the formation of fine grains with a martensite structure in the friction stir processed zone, which led to an important increase of the hardness. The stir processed zone grains became finer when the heat input was lowered. According to the authors, the transverse tensile strength of the friction stir processed zone was equal to that of base material, but all the tensile specimens fractured in the substrate zone. The wear width and depth of the friction stir processed zone, at the load of 1.96 N, were 339 μm and 6 μm, as compared to 888 μm and 42 μm, of the substrate, which corresponds to a decreased of 62% and 86%, respectively. This study also states that low heat input is an effective method to produce FSP zones, with fine grained martensitic structure and improved tensile and wear characteristic.

Aldajah et al. (2009), studied the effect of friction stir processing on the tribological performance of 1080 carbon steel. The process transformed the original pearlite microstructure to martensite, resulting in significant increase in surface hardness. This surface hardening produced a significant benefit for friction and wear behavior of the steel as measured by unidirectional sliding ball-on-flat testing. Under dry sliding, FSP reduced friction coefficient by approximately 25% and wear rate by an order of magnitude. Under oil lubrication, FSP had only a marginal effect on friction, but it reduced wear rates by a factor of 4. The improvement in tribological performance of 1080 steel by FSP technique is attributed to reduced plasticity of the near-surface material during sliding contact.

Grewal et al. (2013), performed surface modification of the 13Cr4Ni hydroturbine steel. In this study the authors analyze the hypothesis of using surface processing in alternative to surface coating, to improve the wear resistance of the hydroturbines. It was found that FSP resulted in the refinement of the microstructure, with reduction in grain size by a factor of 10. EBSD results confirmed the existence of a submicron and ultrafine grained microstructure. The microhardness of the steel was found to enhance by 2.6 times after processing. The processed steel also showed 2.4 times higher resistance against cavitation erosion in comparison to unprocessed steel.

It is important to stress that all the previous studies on FSP of steel were accomplished by using conventional FSW tools, composed by a shoulder with a concentric smaller diameter pin, conducting to relatively thick processing volumes. The first to conduct very thin surface processing, using pinless tools, was Dehghani and co-authors

(Chabok and Dehghani, 2010; Dehghani and Chabok, 2011; Mehranfar and Dehghani, 2011). These authors used a carbide-tungsten shoulder tool, with no pin, to process IF and super austenitic steels. Regarding the surface processing of IF steels, the authors concluded that FSP resulted in the formation of a 30–35 μm thick surface layer, with 50–125 nm nanograins and hardness three times higher than that of the initial substrate hardness. The authors also concluded that increasing the rotating speed, above and below 1600 rpm, resulted in an increase in grain size. The pinless processing of the super-austenitic steel also enabled the production of a 90 μm tick nano-structured layers, with improved hardness, wear resistance and fatigue strength.

In current study a pinless tool, similar to that used by Chabok and Dehghani (2010), was used to perform surface enhancement of S275 and S690 structural steels.

2.2. Slip- resistant joints

According to Kulak et al. (2001), slip-resistant joints, also known as friction-type joints, are bolted joins which have a low slipping probability at any time during the structure's lifetime. Slip-resistant joints are often used in connections subjected to stress reversals, severe stress fluctuations, or in any situation wherein slippage of the structure into bearing would produce intolerable geometric changes. In a slip-resistant joint, the external applied load usually acts in a plane perpendicular to the bolt axis. The load is completely transmitted by frictional forces acting on the contact area of the plates fastened by the bolts. This frictional resistance is dependent on the bolt preload and slip resistance of the faying surfaces. The maximum capacity is assumed to have been reached when the frictional resistance is exceeded and overall slip of the joint occurs that brings the plates into bearing against the bolts.

In the slip coefficient review made by Nah and Kim (2011), it is explained that slip load P_{slip}, depends on the clamping force, T_i, on the slip coefficient, k_s, on the number of slip plates, m, and on the number of bolts in the connection, n. This dependence can be expressed by equation:

$$P_{slip} = k_s mnT_i. \tag{2.1}$$

The slip coefficient, naturally, depends on both steel types and surface treatment.

2.2.1. Surface Treatments

The surface treatments of steels used in structural applications, assume an important role in structural engineering, since those treatments enable to prevent corrosion, promoted by environmental- exposure before the assembly of the structure, and creates a corrosion-resistant layer that reduces the maintenance costs during structure life-time. Although necessary, coatings will decrease the slip resistance of the bolted joins, relatively to the non treated surfaces. However, since those treatments are fundamental for the life of the structure, it becomes important to understand the influence of it in slip resistance.

The first and most widely used coating method to prevent corrosion in structural applications was galvanization, although it application was limited in the case of slip-resistant joins due to the low frictional resistance induced by it in the connections. Meanwhile, new surface treatments started being used for applications where a permanent coating is needed to prevent corrosion and simultaneously increase the joints slip resistance. These surface treatments are classified as hot-dip galvanizing (with or without a preassembly treatment), metalizing (with either sprayed zinc, aluminum, or a combination of both metals), zinc-rich paints (that use organic or inorganic vehicles) and vinyl washes or paints. Texturizing the surfaces, previously to coating, also proved to be one effective way to enhance the slip resistance of the structural components.

2.2.1.1. Hot-Dip Galvanization

This coating technique requires cleaning of the mill scale from the surface prior to coating. The hot-dip galvanization is performed in two steps: the first consist in bathing the structural member in acid, pickling it, and the second consists in dipping it in a hot bath

of metal. The metallic bath is usually pure zinc or iron-zinc alloys. To ensure the corrosion protection, it is important that the galvanized layer presents continuity, which is very difficult to be achieved. The uniformity of the zinc layer also influences the slip resistance, which it was found to decrease by increasing the layer thickness. Actually, the zinc layer behaves like a lubricant between the connected plates. However, it is possible to optimize slip-resistance by using pre-cleaning processes, which increase the roughness of the plate surfaces before hot-dip galvanization. Kulak et al. (2001), studied the influence of several pre-cleaning processes on slip resistance, supporting the results shown in Table 2.1. These author conclude that the sand-blasted surface treatment provides the highest slip coefficient for the hot- dip galvanized surfaces. The other treatments which according them could have some practical use are the phosphate-treatment, the wire-brushing, and the shot-blasting, as well as the acetone-cleaning.

Table 2.1. Summary of Slip Coefficients of Hot-Dip Galvanization Surfaces

Surface Treatment	Slip Coefficient Average	Standard Deviation	Number of Tests
As-received	0,21	0,08	12
Weathered	0,20	0,06	17
Wire-brushed	0,37	0,01	6
Sand-blasted	0,44	0,02	9
Shot-blasted	0,37	0,10	6
Acetone-cleaned	0,32	0,03	9
Phosphate-treated	0,38	0,03	10
Chromate-treated	0,26	0,02	6

2.2.1.2. Metalizing

The metalizing technique also requires roughened free of oil or grease surfaces to improve the adherence of the coating to the surface, being prepared. This process consists in spraying an hot metal, usually aluminum or zinc, on a surface roughened by blasting, in order to provide corrosion resistance. The blast cleaning is usually performed by using sand, crushed slag or chilled iron girt.

According to Kulak et al. (2001), metalizing, in opposition with the hot-dip galvanization, enables achieving high slip resistance. The thickness of the coating has a significant importance in slip resistance, being necessary to optimized it. The hardness of the coating is also very important in determining the slip resistance. It was concluded that aluminum layers provide higher slip resistance than zinc layers, due to the higher aluminum hardness. Usually, in addition to the treatments aiming to improve the corrosion resistance, it is also necessary to apply a sealing treatment. However, this type of treatments reduces the slip resistance because it smoothes the surface.

2.2.1.3. Zinc-Rich Paints

Due to the high content of zinc dust, this type of coatings provides a high resistance to abrasion of the coated members, providing a long-term, to permanent, corrosion resistant applications. These paints could have several components, such as solvents, to control paint viscosity, pigments, to provide color, and vehicles, essential to film layer adhesion to the surface are also needed, (Kulak et al. 2001). There are two types of vehicles, the organic and the inorganic. Meanwhile the organic vehicles can be vinyls, epoxies and polyesters, the inorganic vehicles are mainly silicates, phosphates and its modifications. The inorganic coatings, which are weathering resistant and also resistant to solvents, oil and humidity, should be used over blast-cleaned surfaces. The organic coatings are more flexible to the variations in surface preparation, than inorganic coatings, but they are less tough and abrasion resistant.

According to Kulak et al. (2001), the thickness of the coating layer influences the slip resistance, increasing it. However the chemical content of the paint doesn't have

the same effect. Despite the great range of sleep coefficients, possible to be obtained by varying the application method, the zinc-rich paints always decreases the slip coefficient relatively to the blasted steel surfaces, for any vehicle types.

2.2.1.4. Vinyl Treated Surfaces

Vinyl washes or paints are applied in surfaces previously blasted by sand. As the treatments mentioned before, vinyl washes are also used in corrosion protection of structural members, having significant advantages relatively to the other treatments. Actually, this surface treatment is more easily applied, and cheaper, also providing a good corrosion protection. When the vinyl wash is applied on a sand-blasted surface, the slip resistance, relatively to the non treated surface, it is not so high as for the other processes.

2.3. Materials background

2.3.1. Structural Steels

Structural steels are those currently used in buildings, bridges, ships, off-shore rigs or pipelines. According to ASM Metals Handbook, Vol.1, the structural steels can be divided in four types, as-rolled carbon-manganese steels: as-rolled high- strength low-alloy steels, heat treated carbon steels and heat-treated low alloys steels. In this study were only used a hot-rolled steel and a heat-treated steel, which will be the main subjected of this revision.

### 2.3.1.1. Hot- Rolled Carbon-Manganese steels

The hot-rolled Carbon Manganese steels are usually used in structural shapes as I-beams, channels, wide-flange beams and some special sections. These steels typically have a microstructure composed of dark pearlite islands surrounded by a white ferrite matrix, as shown in the Figure 2.2. The carbon and manganese contents in these steels provide an optimal conjugation of strength, toughness and weldability. Actually, despite the high tensile strength accomplished by increasing the carbon content, the weldability and toughness of the steels becomes reduced. So, in order to increase the strength, without deteriorate the steel toughness, besides increasing the carbon content, the amount of manganese should also be raised.
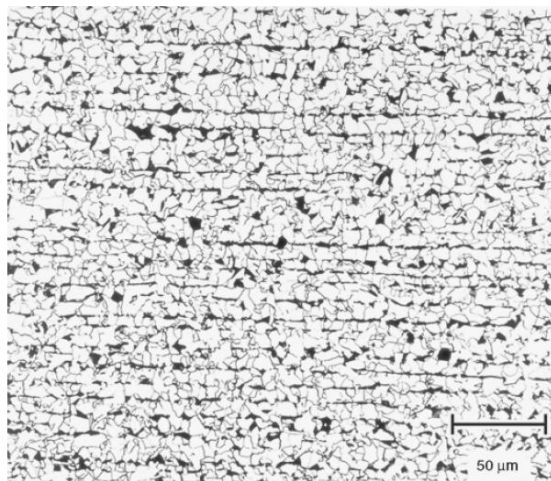
Figure 2.2. Microstructure of an as-rolled micro alloyed steel plate showing equiaxed ferrite grains with bands. Original magnification 200x figure from (ASM International, 2007)

In Figure 2.3 is shown a small extract of the Fe-C phase diagram. In this figure it is exemplified the microstructure evolution, during cooling, for a hypoeutectoid steel, i.e. which has a carbon content lower than 0,77 wt%, when above the M point temperature, riches a homogeneous austenitic microstructure. When in Figure 2.3 the temperature falls below the M point, grains of ferrite start to form. As more grains of ferrite start to form the remaining austenite becomes richer in carbon. At about 723°C the remaining austenite, which now contains 0,77 wt % carbon, changes to pearlite. The resulting structure is a

mixture consisting of white grains of ferrite mixed with darker grains of pearlite, also shown in Figure 2.2.
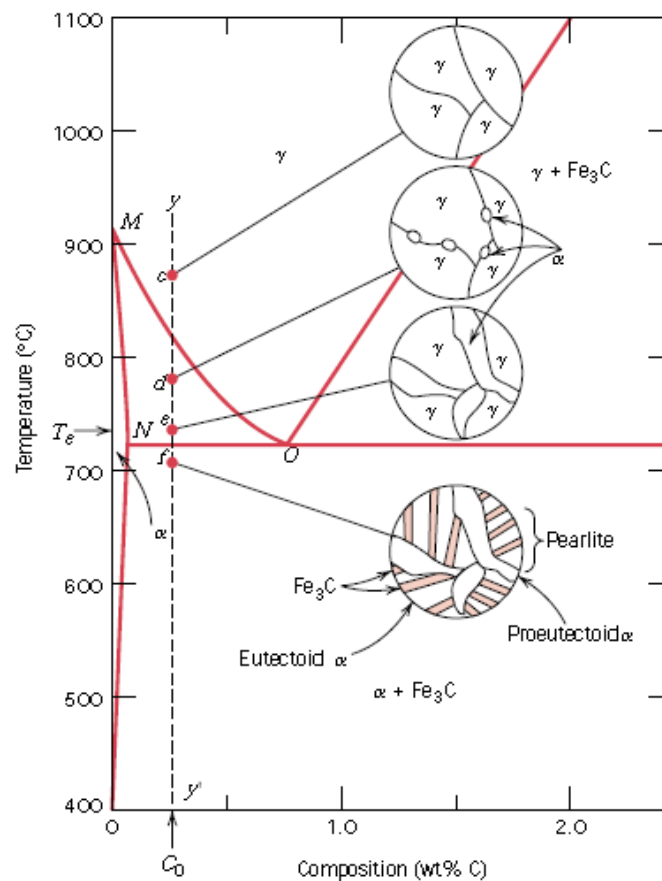

Figure 2.3. Scheme of a part form the diagram phase to the hypoeutectoide steels (Callister Jr, 2001)

2.3.1.2. Heat-Treated Carbon Steels

This type of steels usually, which has yield strength between 290 and 690 MPa, are usually be used in shafts, couplings and to improve the mechanical properties of structural shapes. The heat treatment of these steels could be either normalization or quenching and tempering. The normalization is a process that involves air cooling from autesnitization to room temperatures, producing a ferrite-pearlite structure similar to that studied at previous section, but with a refined grain structure. The more homogeneous and

refined microstructure increases the toughness and strength of the steel relatively to the non treated condition.

On the other hand, in quenching and tempering, the steel is heated to 900ºC, and subsequently quenched in water. After quenching, the material is tempered between 480 and 600ºC, which generates a tempered martensitic or bainitic microstructure, as that exemplified in Figure 2.4. The structures shown in the figure provides a good combination between steel strength and toughness.
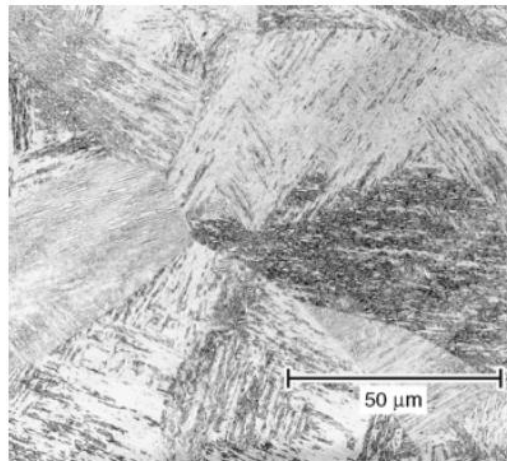
Figure 2.4. Microstructure of quenched low-alloy steel showing delineation of the prior-austenite grain boundaries and lath martensite packets. 2% Nital etch. Original magnification 500x figure from (ASM International, 2007)

[This page intentionally left blank]

[This page intentionally left blank]

3. EXPERIMENTAL PROCEDURE

3.1. Structural Steels

In this work the carbon manganese steel, S275, and the high strength quenched and tempered steel, S690, which the nominal chemical composition are shown in Table 3.1, were subjected to FSP.

Table 3.1. Nominal chemical composition (wt%)

Material	C	Mn	P	S	N	Cu	Si	B
S275	0,24	1,6	0,045	0,045	0,014	0,60	---	---
S690	0,22	1,8	0,030	0,017	0,016	0,55	0,86	0,006
Material	Cr	Mo	Nb	Ni	Ti	V	Zr	Fe
S275	---	---	---	---	---	---	---	rem
S690	1,6	0,74	0,07	2,1	0,07	0,14	0,17	rem

3.2. Friction Stir Processing

Friction stir processing (FSP) was carried out using the MTS I-STIR PDS equipment shown in Figure 3.1 (a), at AIMEN, in Spain. Two WC-Co columnar FSP tools, with shoulder diameters of 16 and 20 mm, and no pin (as is shown in Figure 3.1 (b)), were used for processing the S275 steel. The S690 base material was processed using the 16 mm

diameter tool. FSP was accomplished in position control, using a 2° tool tilt angle (α) and 0.3 mm penetration into the substrate plates. In order to analyse the influence of the tool rotation and traverse speeds, on processing results, these two process parameters were varied, for each substrate, according to Table 3.2. Argon gas was used for surface shielding during FSP.
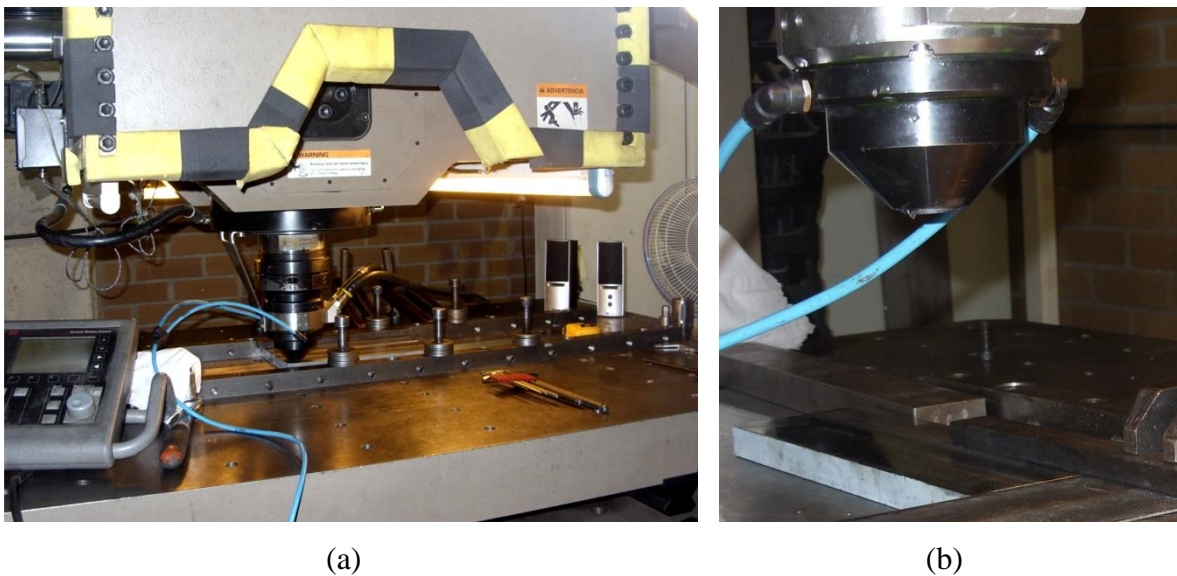

(a)   (b)

Figure 3.1. MTS I-STIR PDS equipment (a); and pinless tool (b)

Table 3.2. Process Parameters

Material	Tool Diameter [mm]	Travel Speed [mm/min]	Rotation Speed [rpm]
S275	20	250	200-500
	16	250-550	300-500
S690	16	250-550	300-600

3.3. Metallographic Analyses

After processing all the samples were visually inspected and photographed, with a Canon Powershot G5 camera, using a 5x magnifying glass, in order to classify the quality of the processed surfaces. The processed samples were then sectioned, transverse to the FSP direction, and mounted in self-curing resin. All the samples were mechanically polished, using metallographic carbon silicate sandpaper with decreasing granulometry (P180, P600, P1000 e P2500). Final polishing was performed using 3 micron diamond suspension. Etching was then performed for 30s, with Nital solution (2ml HNO_3 + 98ml ethanol (95%)) (Geels et al. 2007). The microstructure of the processed zones was examined by optical microscopy (OM) using ZEISS Axiotech 100HD microscope, with magnifications of 50x, 100x, 200x, 500x and 1000x. Both the magnifying glass and the optical microscope can be seen in Figure 3.2 (a) and (b), respectively.

(a)   (b)

Figure 3.2. Magnifying glass (a); Optical light microscope (b)

3.4. Hardness Tests

The hardness of the processed surfaces was measured using Vickers macro-indentation, under a 98 N load, for the BM, and Vickers micro-indentation, under 1,96 N, for the processed surface. The load holding time was 15 s in all cases. Several microhardness tests were performed, perpendicularly to the samples surfaces, in the center of the processed samples. In each testing line the hardness measurements were spaced by intervals of 250 µm.

Vickers Hardness was calculated using the arithmetic average of the diagonal, d_{HV} (in mm), and the test load (in kgf), P, according to the equation:

$$\mathbf{HV} = \frac{1,8544P}{d_{HV}^2}$$

(3.1)

3.5. Friction Tests

Measurements were carried out for static friction coefficients, for surface roughness conditions corresponding to a processed surface and a polished surface finishing. Due to some problems in samples machining, only one processed surface was tested, corresponding to the S275 steel.

The friction measurement device used in this study, shown in Figure 3.3, is an original equipment developed at CEMUC. The setup was mounted on a standard tensile testing machine equipped with a 10 kN load cell with electronic control of the motion of the cross- head of the testing machine. In the experiments a normal force (F_N=2000 N) was applied between three bodies in contact: an AISI 1045 steel counterbody and the two surfaces being tested, as shown in Figure 3.4. During testing the sliding friction was generated at the counterbody/samples interface by displacing the counterbody at a constant speed of 5 mm/min. The tests were carried out at room

temperature in dry conditions and for a sliding displacement of 5 mm. In order to check the reproducibility of the results, two sets of tests were carried out for each sample.

Figure 3.3. Samples support equipment of the friction tests
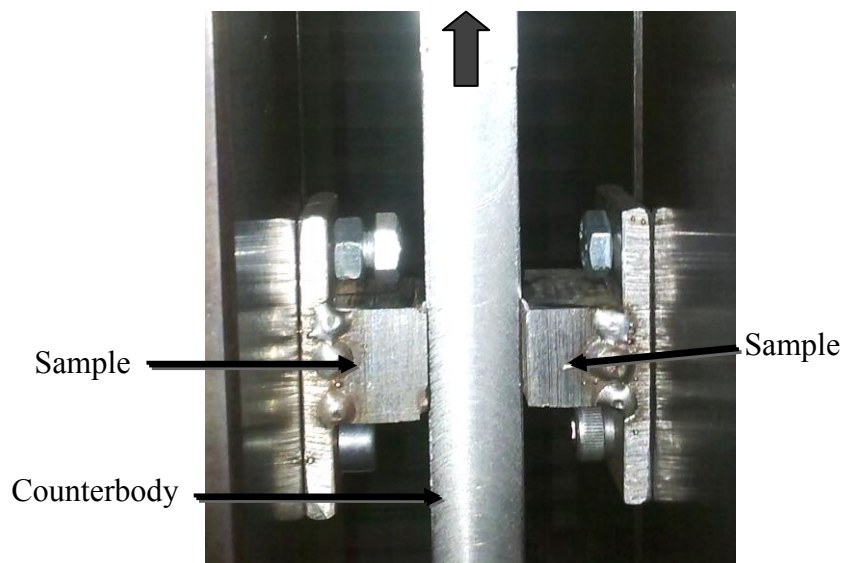
Figure 3.4. Samples and matrix assembly of the friction tests

[This page intentionally left blank]

[This page intentionally left blank]

4. RESULTS AND DISCUSSION

4.1. Visual Inspection

All the surfaces obtained by FSP were visually inspected in order to characterise the evolution of the surfaces morphology with varying processing parameters. In Table 4.1 and Table 4.2 are shown images of the processed surfaces for the S275 and S690 steels, respectively.
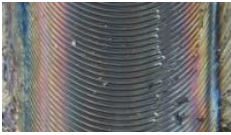
In Table 4.1, where are shown the results for the S275 steel, it is possible to see the evolution with process parameters of the morphology of the surfaces produced with the 20 and 16 mm diameter tools. For the 20 mm diameter tool are shown the surfaces obtained by varying the tool rotation speed from 500 to 200 rpm, at a constant traverse speed of 250 mm/min. For 16 mm diameter tool are shown the surfaces obtained by varying the tool rotation speed from 500 to 300 rpm at a constant traverse speed of 250 mm/min, and the surfaces obtained when processing at a constant tool rotation speed of 500 rpm and traverse speeds varying from 250 to 550 mm/min. Analyzing the images it is possible to depict, in each surface, the arc shaped striations characteristic of any friction stir processed/welded surface. It is well known that the number of striations, or shoulder marks, per millimetre, is proportional to the ω/v rate, increasing when rotation speed increases, for a constant tool traverse speed, and when the traverse speed decreases, for a constant tool rotation speed. The evolution in the striation number, per millimetre, can be observed by comparing the images in the table.

Comparing the surfaces obtained for the 20 and 16 mm tools, at a constant traverse speed of 250 mm/min and increasing tool rotation speeds, it is possible to conclude that for the lower tool rotation speed of 200 rpm, for the 20 mm diameter tool, and 300 rpm, for the 16 mm diameter tool, both surfaces display irregular striations with very low depth which can be attributed to a very low heat input during processing. Actually, when increasing the tool rotation speed, which is the main parameter in determining the heat generation during processing, the striations became much more
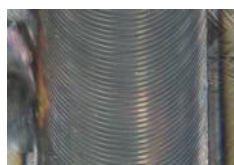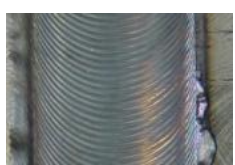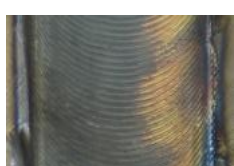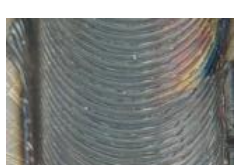
regular and well defined. The same is true when processing at the higher tool rotation speed of 500 rpm and increasing tool traverse speeds, as is possible to conclude by analysing the 16 mm diameter tool surfaces. Another important difference between the surfaces obtained with both tools is the presence of some flash irregularities in the middle of the processed area for the 20 mm diameter tool surfaces, which can be attributed to a higher heat input during processing and/or to the utilization of inappropriate tool tilt angle for this tool. For most of the samples it was also observed the formation of flash in both sides of the processed surface. The presence of flash, in the middle or at both sides of the processed path can have an important influence on the friction behaviour of the surfaces. These irregularities are also unhallowed when it is intended to process large surfaces by overlapping multiple processing passes.

Analysing now Table 4.2, where are shown the processed surfaces obtained for the S690 steel, using the 16 mm diameter tool and almost the same range of processing parameters that were used for processing the S275 steel, it is possible to conclude that the S690 surfaces display almost the same macro features of the S275 surfaces. However, unlike for the S275 steel, for this material it was possible to obtain a regular surface morphology when processing at 300 rpm. It is also possible to observe that the S690 steel surfaces display a lower amount of flash than the S275 surfaces. Actually, for the S690 steel, large amounts of lateral flash were only observed when processing at 600 rpm, which corresponds to the higher heat input conditions of all the tests performed for both alloys.

Table 4.1. Visual inspection of S275 samples

S275	ω \ v	250 [mm/min]	350 [mm/min]	450 [mm/min]	550 [mm/min]
20 mm	500 [rpm]				
	400 [rpm]				
	300 [rpm]				
	200 [rpm]				
16 mm	500 [rpm]				
	400 [rpm]				
	300 [rpm]				

Table 4.2. Visual inspection of S690 samples

S690 / ω \ v	250 [mm/min]	350 [mm/min]	450 [mm/min]	550 [mm/min]
600 [rpm]				
500 [rpm]				
400 [rpm]				
300 [rpm]				

(16 mm)

As shown in the previous analyses, the ω/v ratio is an important factor in determining the surface morphology of processed samples, since it simultaneously determines the number of striations per millimetre, which will have an important influence in the friction behaviour of the surface, as well as in the heat generation during the process. The heat input during the process has a strong influence on the quality of the surface, as well as on the microstructural evolution of the processed material.

4.2. Spindle Torque Analysis

In order to provide a better insight on the relation between the ω/v ratio and heat generation during processing, a torque sensitivity analysis was performed. According to Khandkar et al. (2003) and Pew et al. (2007), the torque registered during processing is a suitable parameter for evaluating the heat input during the process. In Figure 4.1 is plotted, for both steels, the average torque registered during processing as a function of the ω/v ratio. The spindle torque values plotted in the figure were directly obtained from the FSP equipment. In the figure are also plotted lines representing the evolution of the torque with the rotation speed, determined by fitting the equation

$$\tau = a \times \omega^{-b}$$

(4.1)

to the torque results. In this equation *a* and *b* are constants, which according to Leitão et al. (2012), depend on the processing parameters and processed material characteristics. In order to facilitate the interpretation of the figure, in table 4.3 are represented the tool traverse and rotational speed corresponding to each ω/v ratio.

Analyzing Figure 4.1 it is possible to conclude that, independently of the processed steel and processing conditions, for a constant traverse speed, the torque values strongly decrease with increasing rotational speed. For a constant rotational speed and varying traverse speed no important changes in torque were registered, as can be depicted from the figure, where horizontal lines were used for fitting these results. According to Arora et al. (2009), increasing the tool rotation speed, increases the temperature, decreasing the flow stress associated to material stirring during the process, which decreases the spindle torque, as registered in the figure. Arora et al. (2009), also reported that the torque is relatively insensitive to the traverse speed, since this parameter does not affect the heat generation during processing, having only influence on the heating and cooling rates.

Comparing in Figure 4.1 the torque results relative to the S275 steel it is also possible to conclude that the torques registered when processing with the 20 mm diameter tool are much higher than that registered when processing with the 16 mm diameter tool. This indicates that the amount of material dragged by the tool at each rotation is higher for

the 20 mm than for the 16 mm diameter tool. In the same way, it is also possible to conclude that, for the 16 mm diameter shoulder, the torque values registered when processing the S690 steel are higher than that registered when processing the S275 steel. This is related with the higher strength of the S690 steel, relative to the S275, which necessarily increases the energy required for processing.
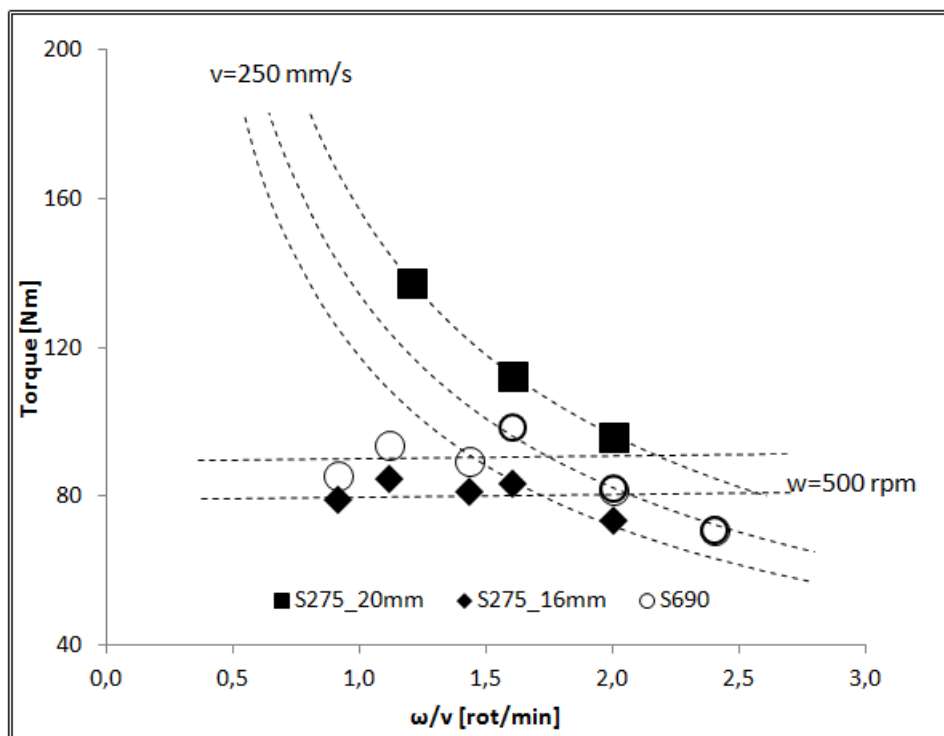

Figure 4.1. Process Parameters Influence on Torque

Table 4.3. Legend ω/v ratio

ω/v Ratio [rot/mm]	ω [rpm]	v [mm/min]
0,9	500	550
1,1	500	450
1,2	300	250
1,4	500	350
1,6	400	250
2,0	500	250
2,4	600	250

4.3. Metallographic Analysis

In Figure 4.2 are shown micrographs which represent the microstructures of the S275 (Figure 4.2 (a)) and S690 (Figure 4.2(b)) substrates. In Figure 4.2 (a) it is possible to depict the well known ferrite-pearlite microstructure characteristic of C-Mn hot-rolled steels. The microstructure in Figure 4.2(b) displays microstructural features, which, according to the literature, should correspond to the presence of the Martensitic or Bainitic structures characteristic of quenched and tempered steels.

In order to highlight the microstructural changes induced by FSP on the substrate materials, in Figure 4.3 and Figure 4.4 are shown macrographs of the processed surfaces for the S275 and S690 steels, respectively. These images correspond to the samples processed at the maximum tool rotation speed and the minimum traverse speed for each substrate. In both figures, it is possible to see a different contrast in the stir zone indicating that some microstructural changes occurred inside of it. For the S275 sample it is even possible to distinguish under the darker processed zone, another area, with different contrast of that on base material, which should correspond to the Heat Affected Zone. The HAZ is not discernible for the S690 sample.

Microstructural evolution from the processed surface, to the unaffected substrate, for the rest of the samples, was found to be similar to that shown in Figure 4.3 and Figure 4.4 for the S275 and for the S690, respectively. For this reason no images of the other samples were included in the text.
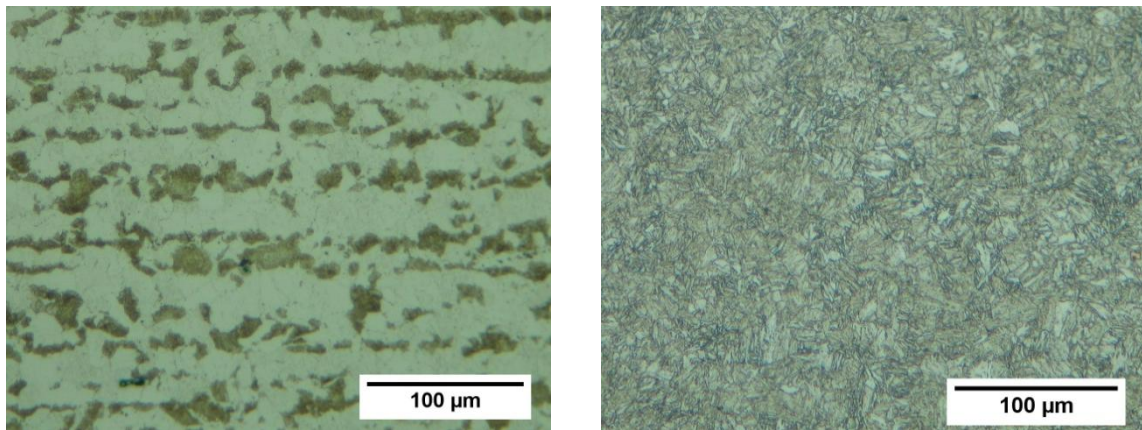
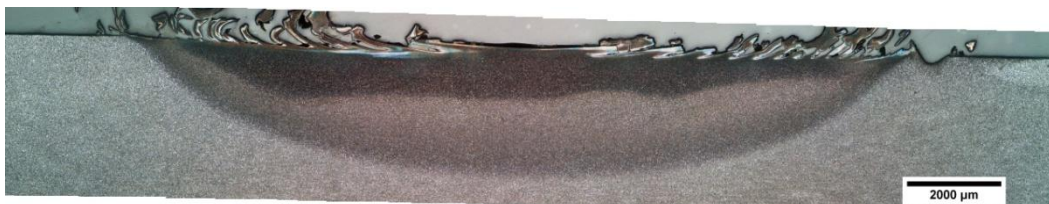(a)   (b)

Figure 4.2. Substrate microstructures: S275 (a); S690 (b)

Figure 4.3. Macrographs of S275 steel

Figure 4.4. Macrographs of S690 steel

4.4. Mechanical Properties

4.4.1. Hardness Tests

In order to evaluate the evolution in the mechanical strength of the stirred zone relative to the substrate, hardness measurements were performed, across the processed zone, according to the procedure described in Chapter 3. The hardness profiles obtained for some selected samples are shown from Figure 4.5 to Figure 4.9. In Figure 4.5 and Figure 4.6 are shown the hardness profiles corresponding to the S275 samples processed with the 16 mm and 20 mm diameter tools, respectively, using the maximum tool rotation speed of 500 rpm, and the minimal tool traverse speed of 250 mm/min, i.e. using the higher heat input conditions of all tests performed for this material. Comparing both figures it is possible to conclude that the depth of the processed zone is slightly higher for the 20 mm diameter tool. Instead of that, the profile shapes are similar denoting an increase of hardness in the processed zone relative the unprocessed substrate. It is also possible to see in both figures a hardness peak in the lighter coloured zone previously identified as HAZ.

In Figure 4.7 is shown another hardness profile corresponding to the S275 steel, processed with the 20 mm diameter tool, but now using the lowest value of tool rotation speed, which corresponds to a lower heat input during processing. Comparing these results, with that in Figure 4.6, it is possible to conclude that decreasing the tool rotation speed from 500 rpm to 300 rpm, the depth of the processed zone decreased significantly, as well as the maximum hardness values registered inside this zone. A hardness peak in the HAZ can also be observed in the profile of Figure 4.6.

In Figure 4.8 and Figure 4.9 are now compared the hardness profiles registered for the S690 samples, processed at 500 rpm and traverse speeds of 250 mm/min and 550 mm/min, respectively. Both figures show an important hardness increase, relative, to the initial substrate hardness. Contrarily to that registered for the S275 steel, no hardness peak can be seen in the HAZ of the S690 samples. The main difference between both S690

samples is the processed zone depth, which clearly diminishes when the tool traverse speed is increased.

The hardness profiles for the other samples processed in this work, which were not included in this graphic, display the same features of that shown in Figure 4.5, Figure 4.6 and Figure 4.7, for the S275 steel, and in Figure 4.8 and Figure 4.9, for the S690 steel.

Figure 4.5. Example of hardness evolution S275 sample processed using the 16 mm diameter tool

Figure 4.6. Example of hardness evolution S275 sample processed using the 20 mm diameter tool

Figure 4.7. Example of hardness evolution S275 sample processed using the 20 mm diameter tool
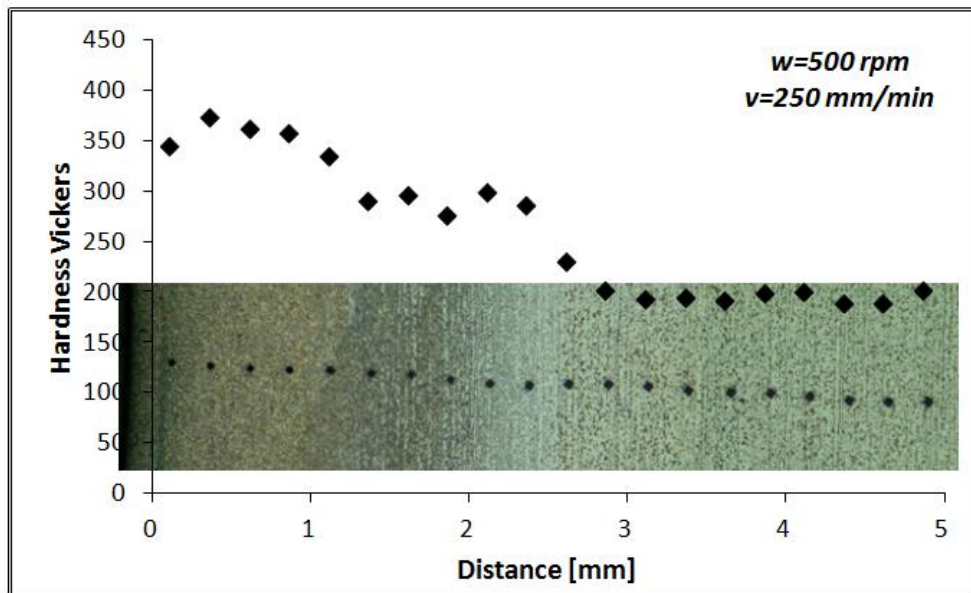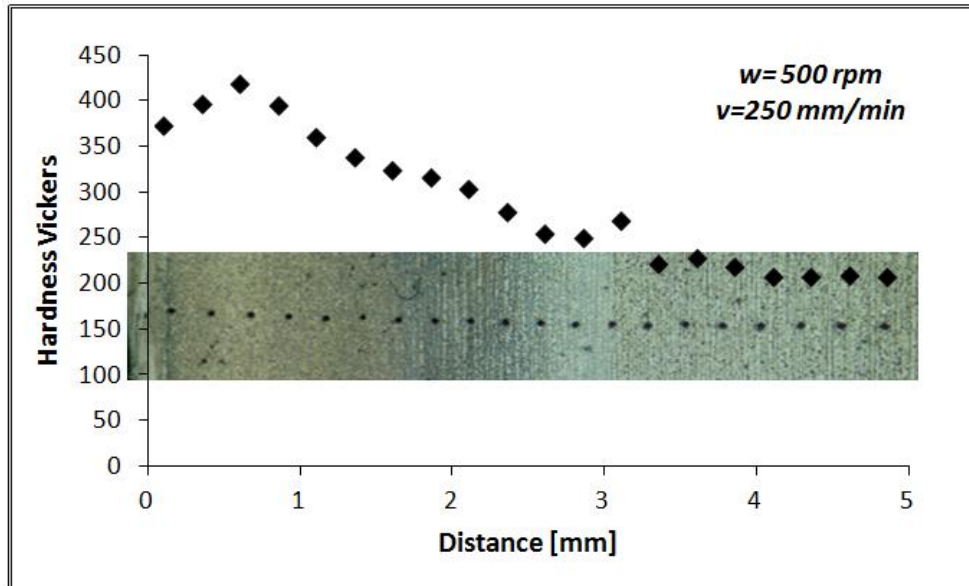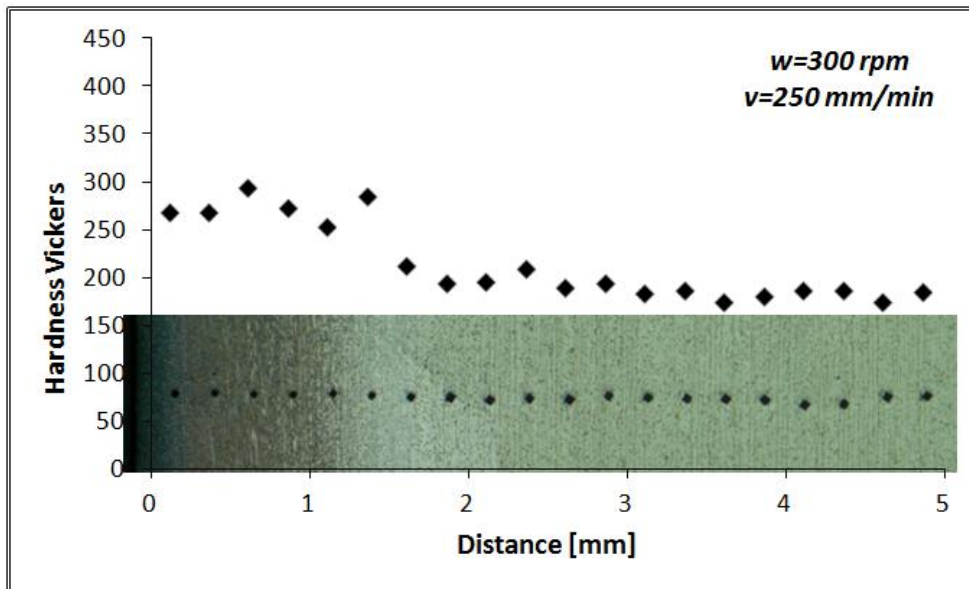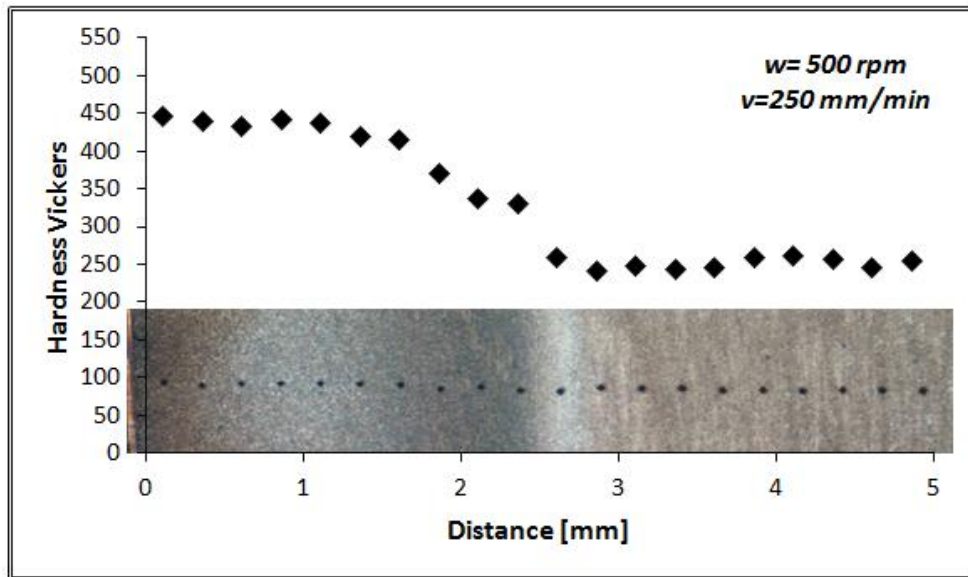
Figure 4.8. Example of hardness evolution S690 sample processed using the 16 mm diameter tool
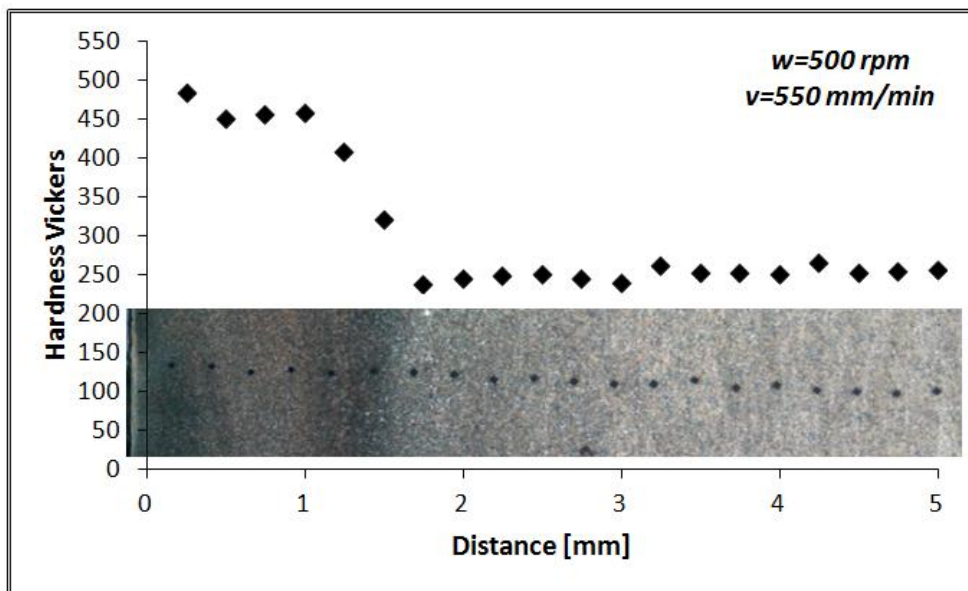
Figure 4.9. Example of hardness evolution S690 sample processed using the 16 mm diameter tool

In Figure 4.10 and Figure 4.11 are now plotted the maximum hardness values registered for all the samples processed. This maximum hardness values correspond to the average of the hardness values registered in the first millimetre depth of each profile. The hardness results are plotted as a function of the tool traverse speed, in Figure 4.10, and as a function of the tool rotation speed, in Figure 4.11. In both figures are plotted lines corresponding to the average hardness of the substrates (200 HV and 265 HV for S275 and S690 steels, respectively).

Analyzing Figure 4.10, where are plotted the hardness values obtained for the samples processed at increasing values of tool traverse speed, and at a constant tool rotation speed of 500 rpm, it is possible to conclude that the hardness of the samples doesn't vary significantly when varying the tool traverse speed. The only exception is registered for the S690 steel, for which there is a slight increase in hardness when increasing the traverse speed from 250 to 350 mm/min.

The average hardness increase (ΔHV) in the processed zones, relatively to the substrate, was of 180 HV, for the S275 steel, and of 238 HV, for the S690 steel, which corresponds to a 90% hardness increase for both materials.
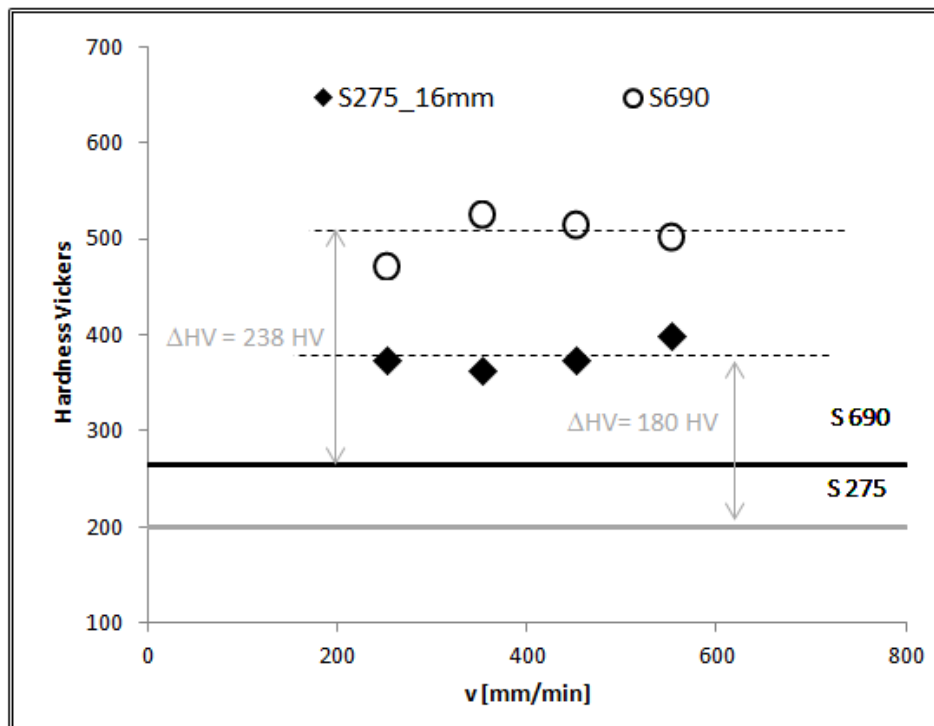
Figure 4.10. Influence of tool traverse speed on hardness (ω=500 rpm)

Analyzing now Figure 4.11 where is plotted the evolution of the processed zones hardness with increasing tool rotation speeds, for a constant tool traverse speed of 250 mm/min, it is possible to conclude that for the S690 steel, no important hardness variations were registered by changing the tool rotation speed. On the other hand, for the S275 steel, it is possible to observe an increase in hardness when increasing the tool rotation speed from 300 to 500 rpm. It is also possible to conclude that the hardness of the processed samples didn't change when changing the tool diameter from 16 to 20 mm, which indicates that the heat input during processing was similar for both tools.
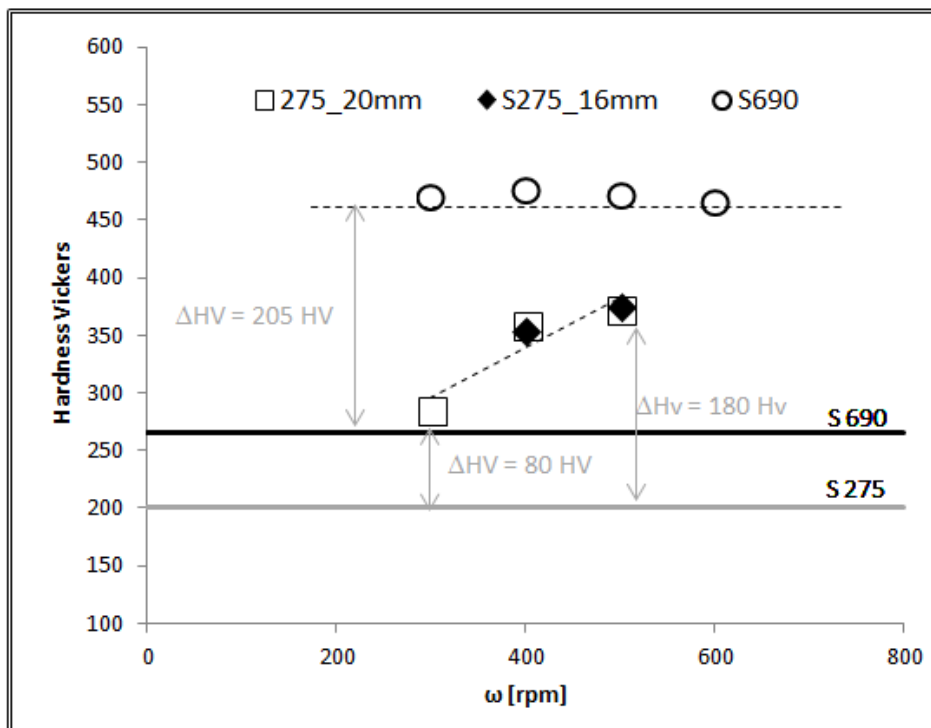
Figure 4.11. Influence of tool rotation speed on hardness (v=250 mm/min)

Analyzing the hardness results displayed in this section, it is possible to conclude that the average hardness of 200 HV, registered for the S275 steel, is higher than that expected for a 275 MPa yield strength steel. However, since the processed samples resulted from the sectioning of very large specimens tested in tension by ISISE, it is expected that the resulting microstructure display a plastically deformed structure with higher hardness than the non-deformed material. After processing, at different tool rotation speeds, important hardness increases were registered in the stirred zones of this steel. The hardness varies from 280 HV, for the samples processed under the lower heat input conditions (ω=300 rpm), to 380 HV, for the samples processed under the higher heat input conditions (ω=500 rpm). This hardness increase can be attributed to the stirred zone grain size refinement, reported in the microstructural analyses, as well as to the formation of brittle structures inside this area as a result of the severe thermal cycles experienced during processing.

In order to analyse the possible influence of the grain size refinement on the hardness evolution, in Figure 4.12 are plotted curves representing the evolution of hardness versus grain size obtained by applying the well known Hall-Petch relation

$$H = H_0 \times k_h d^{-1/2}$$

(4.2)

where H_0 and k_h are constants and d is the grain size for the material hardness. In the graph are also signalized the maximum hardness limits registered for both steels, for the varying processing conditions. Analysing in the figure the results relative to the S275 steel, it is possible to see that for a hardness variation from 280 HV to 380 HV, the grain size should decrease from around 8,5 µm to 2,5 µm. However, it is important to point that, according to Figure 4.11 the higher hardness was registered for the sample processed at 500 rpm, i.e. for the higher heat input conditions, which necessarily corresponds to the coarser grain structure. In this way, the evolution in hardness registered when processing at increasing tool rotation speeds can't be only related to grain size, but has to be also related to the formation of brittle structures during the cooling of the processed materials. In this way, the hardenability of the S275 steel was evaluated by calculating the carbon equivalent

$$C_{eq} = \%C + \frac{\%Mn}{6} + \left(\frac{\%Cr + \%Mo + \%V}{5}\right) + \left(\frac{\%Cu + \%Ni}{15}\right)$$

(4.3)

using the chemical nominal composition of the steel shown in Table 3.1. It was obtained C_{eq}=0,54, which indicates that the steel has a high hardenability.

In Figure 4.13 is shown a graphic which indicates the hardness associated to the different microstructures that can be formed during cooling of structural steels. For the carbon content of the S275 steel, according to the graphic, a hardness of 380 HV corresponds to the formation of martensite, meanwhile the lower hardness of 280 HV corresponds to the formation of ferrite, pearlite and bainite. In this way it is possible to assume that the hardness variation registered for the S275 steel, at increasing tool rotation speeds, results from the conjugated effect of grain size refinement, with the formation of different structures, as a result of the evolution of the peak temperatures with tool rotation speed. Evidences of the evolution of the heat input with process parameters were provided in the torque sensitivity analyses of Figure 4.1.

For the S690 steel no important differences in hardness were registered when processing at different tool rotation speeds. The only evolution in hardness that can be reported for this steel corresponds to the hardness increase registered between the samples processed at 250 mm/min (Figure 4.11) and that processed at traverse speeds equal or higher than 350 mm/min, i.e. when increasing the heating and cooling rates during processing. However, in any case, hardness increases, relative to the unprocessed substrate, of 80% to 90%, were always registered. Again, this hardness increase has to result from the combined effect of grain refinement and the formation of brittle structures. According to the Hall-Petch relation for this steel, a hardness variation between 470 and 500 HV corresponds to very small grain size differences. The carbon equivalent for this steel is also very high (C_{eq}=1,2), indicating that this material has a very high hardenability, being susceptible to embrittlement for a large range of processing conditions, which may explain the small variations in the hardness reported in this work for the S690 processed surfaces.
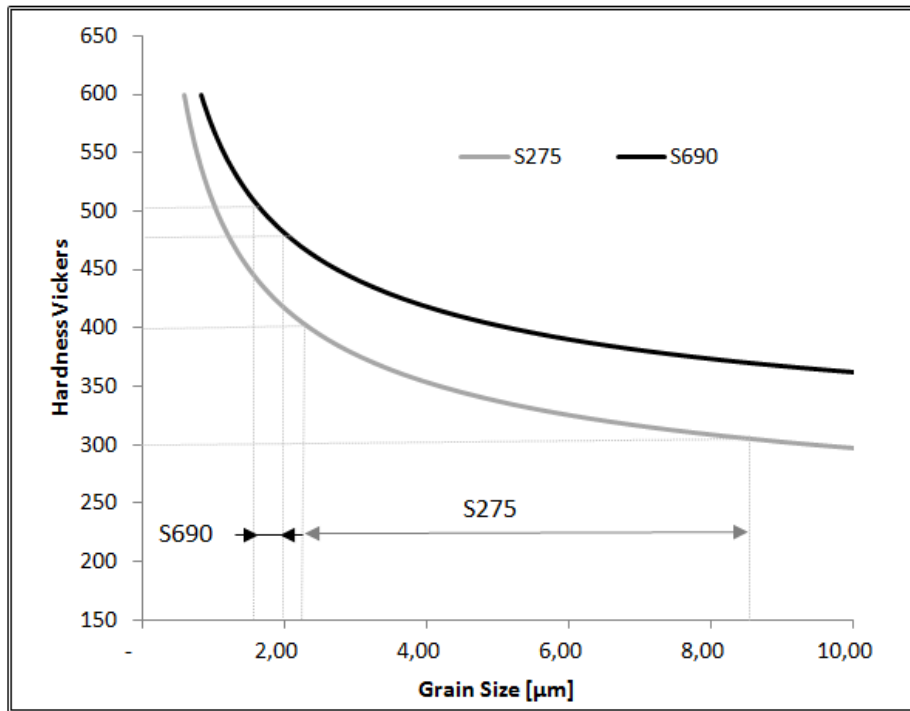
Figure 4.12. Hardness vs grain size according to Hall-Petch relation
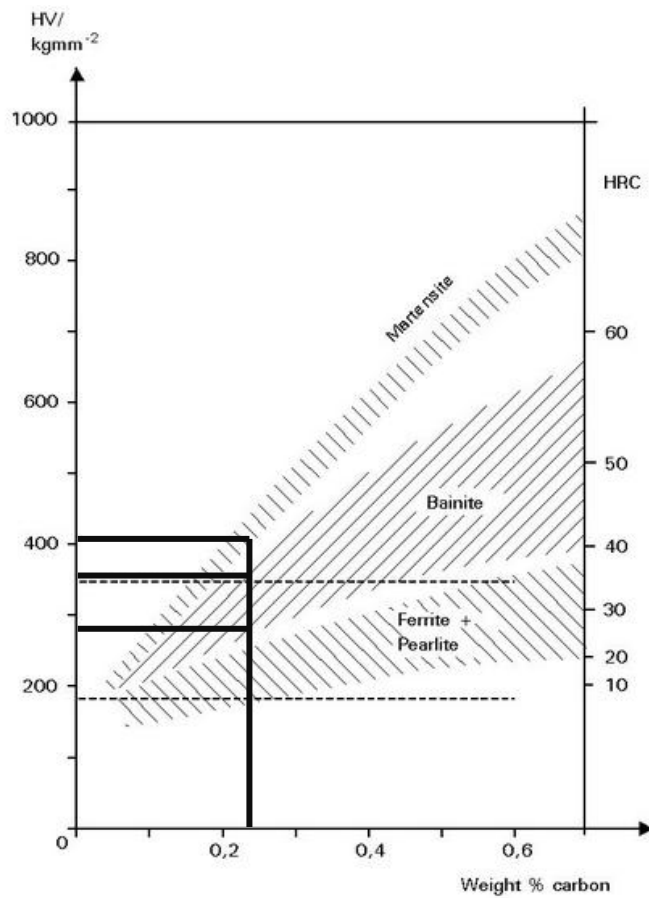
Figure 4.13. Effects of carbon content on the hardness of various structural steel micro-structures (Ljubljana U.)

4.4.2.   Friction Tests

In Figure 4.14 and Figure 4.15 are shown the forces recorded during the friction tests of the processed (FSP results) and unprocessed samples (BM results). The force-displacement curves show two distinct stages. In the first stage the counterbody did not slip on the samples and the tangential force increases almost linearly as a function of time, until a maximum tangential force value is reached. During this stage, due to the stiffness of the tensile machine, the stiffness of the testing equipment, as well as the nature of the contact between the counterbody/samples surfaces, only elastic deformation takes place. The second stage starts after the maximum tangential force is achieved, when the counterbody started sliding against the samples. As is possible to see in both graphs, during this second stage, the force is not constant. However, since only the determination of static friction coefficients and assembly stiffness, are intended in current work, this part of the curves has no specific interest. Using the data in Figure 4.14 and Figure 4.15, the static friction coefficient (μ_s) was calculated based on Coulomb's law

$$\mu_s = \frac{F_T}{2 \times F_N} \qquad (4.4)$$

in which F_T is tangential force and F_N is the normal force applied by the clamping system to each sample. The tangential force value used to determine μ_s is estimated from the first stage of the recorded curves, corresponding to the first maximum value of the force in each curve.

Figure 4.14. Tangential force vs displacement registered during friction tests of unprocessed surfaces

Figure 4.15. Tangential force vs displacement registered during friction tests of processed surfaces

Table 4.4. Static friction coefficients and stiffness for each test

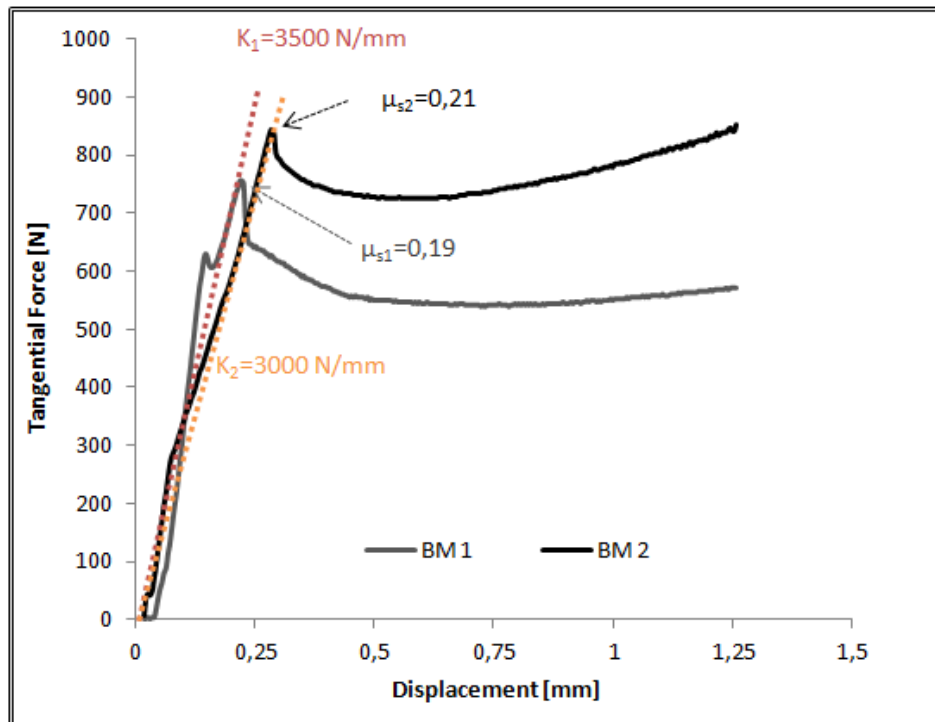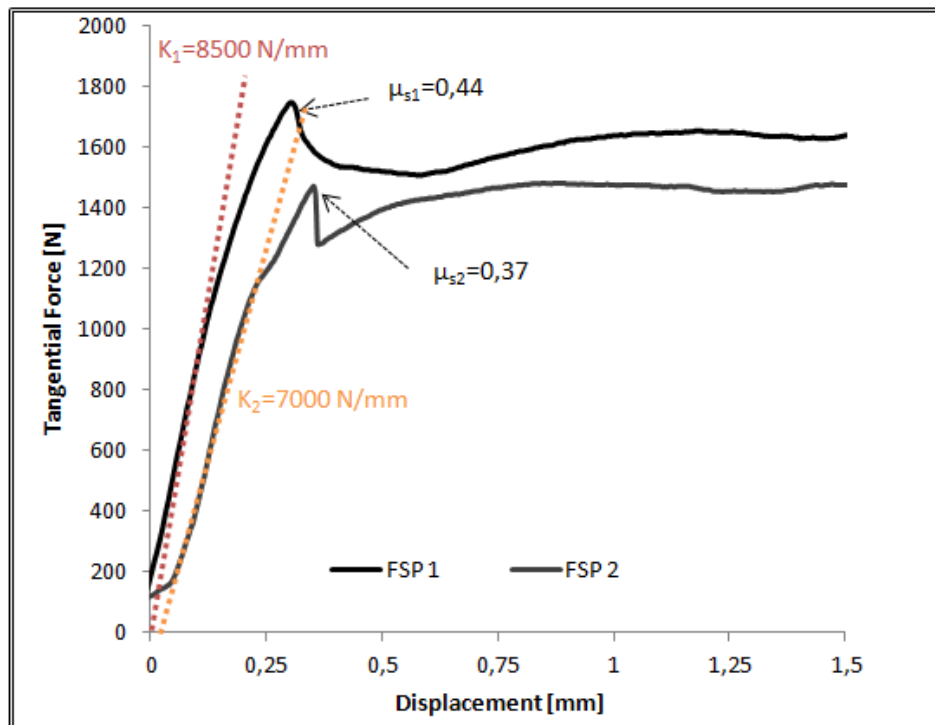| BM 1		BM 2		FSP 1		FSP 2	
μ_s	K	μ_s	K	μ_s	K	μ_s	K
0,19	3500	0,21	3000	0,44	8500	0,37	7000

In Table 4.4 are shown the static friction coefficients determined using the data in Figure 4.14 and Figure 4.15. Analysing the results it is possible to notice some variations in the friction coefficients, for both the processed and unprocessed samples. The differences in the static friction coefficient for the unprocessed samples may result from changes in surface conditions, such as cleaning and roughness. In fact, since both the counterbody and the samples are ferritic- pearlitic steels, with high ferrite- α content, the friction behaviour of the samples will depend on the occurrence of localized micro-adhesion between the surfaces, promoted by the high solubility of the ferrite-α of both surfaces in contact. In Figure 4.16 (a), where is shown an image of the surface of one of the unprocessed samples, it is possible to observe the wear marks resulting from the phenomenon described above.

The friction behaviour reported for the processed samples depends on different mechanisms from that governing the friction behaviour of the unprocessed surfaces. In this case the friction behaviour of the interface is governed by the anchorage resulting from the penetration of the very hard striations, of the processed surfaces, in the softer counterbody material. This penetration will promote the plastic deformation of the material, trapped between the striations, increasing the necessary load for sliding. Since the roughness across the processed surface is not constant, the friction coefficient determined in both tests display some variations. In Figure 4.16 (b), where is shown an image of the surface of one of the processed samples, it is not possible to observe any relevant marks resulting from the wear or plastic deformation of the striations during the friction test.

<div align="center">(a)   (b)</div>
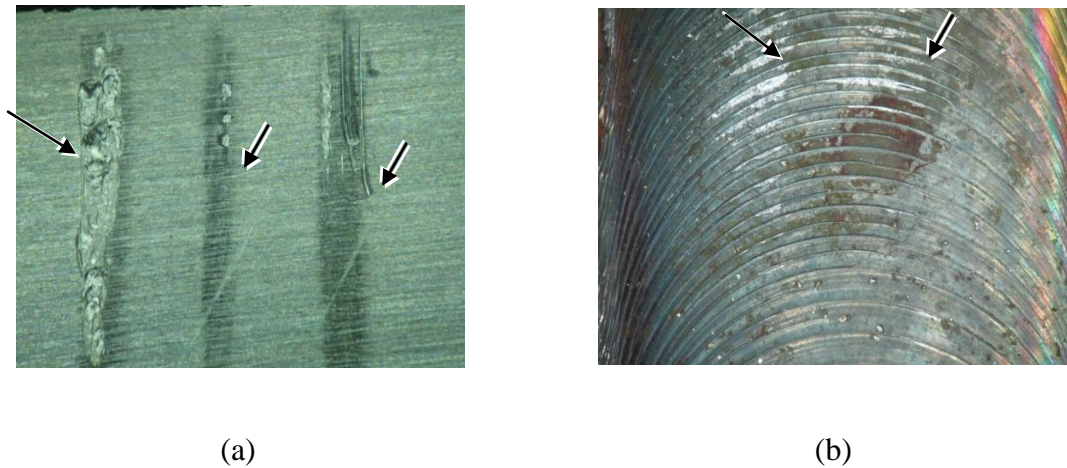
Figure 4.16. Wear marks after friction tests: Unprocessed material (a); Processed material (b)

For both FSP and BM samples, the scattering in static friction coefficient results could be minimized by realizing more tests. However, in any case, it is important to stress that the friction coefficient determined for the processed surfaces is double of that registered for the unprocessed surfaces.

Another important conclusion from Figure 4.14 and Figure 4.15 is that the stiffness was drastically increased when testing the processed surfaces. Actually, the stiffness values presented in the figures, and inTable 4.4, for the processed samples tests are double of that registered for the unprocessed samples.

[This page intentionally left blank]

[This page intentionally left blank]

5. CONCLUSIONS

In this work it was studied the influence of the processing conditions on the surface enhancement/texturing of two structural steels, an hot rolled carbon-manganese steel (S275) and a quenched and tempered steel (S690). The surface morphology, the microstructure and the mechanical properties of all the processed samples were analysed and compared.

From this work it was possible to conclude that, when processing the S275 steel at the lowest tool rotation speed, independently of the tool diameter, the heat input was insufficient to promote the material softening necessary to promote plastic deformation in a suitable depth. Increasing the tool rotation speed, for the lower diameter tool, it was possible to obtain non-defective surfaces with regular and well defined striations. However, when increasing the tool diameter, the processed surfaces started displaying a non-uniform flash randomly distributed in the middle of the processing track. These surface irregularities are believed to be detrimental for the friction behaviour of the surfaces, since it will obstruct the perfect contact of the surface with any counterbody. After evaluating the surfaces microstructure and hardness it is also possible to conclude that flash formation has to result from the use of an inappropriate tool tilt angle (α=2º). Actually, no important differences in hardness were reported for the samples processed with different diameter tools, when using similar tool rotation and traverse speeds, which indicates that no important differences in heat generation could have occurred when processing with the different tools. On the other hand, when processing the S275 steel with the lower diameter tool and increasing tool rotation speeds, important variations in hardness were reported. The hardness of the surfaces was observed to increase by increasing the tool rotation speed. No variations in hardness were reported by changing the processing speed. These results indicate that the metallurgical transformations occurring during the processing of the S275 steel are governed by the peak temperature reached during processing, which depends on tool rotation speed, and independent of the heating and cooling rates, which depends on tool traverse speed.

The S690 processed surfaces, obtained using the lower diameter tool and the same processing parameters used to process the S275 steel, showed to be very regular even

for the very low tool rotation speed that proved to be ineffective for the processing of the S275 steel. Contrarily to that registered for the S275 steel, no important differences in hardness were registered when processing the S690 steel at increasing tool rotation speeds, even when using an extreme value of rotation speed of 600 rpm. The only difference in hardness was registered for the surface processed at the lower tool rotation speed, showing that metallurgical transformations occurring during processing, for this material, are sensitive to the heating and cooling rates promoted by the process. For both steels, it was also possible to conclude that an important hardness increase, of around 90%, took place for all the stirred zones after processing. These hardness increase was associated to the grain refinement of the processed material and to the formation of brittle structures during cooling.

Finally considering the friction tests preformed, it is possible to conclude that the processed surfaces displayed static friction coefficients double than that registered for the unprocessed surfaces. Processing also promoted the creation of a stiffer connection with the AISI 1045 counterbody. Based on these results, it is possible to conclude that FSP could be a suitable surface texturing technique for the enhancement of non-sliding connections.

REFERENCES

Albakri, A. N., Mansoor, B., Nassar, H., & Khraisheh, M. K. (2013): *Thermo-mechanical and metallurgical aspects in friction stir processing of AZ31 Mg alloy — A numerical and experimental investigation*, Journal of Materials Processing Technology, Vol. 213, pp. 279–290.

Aldajah, S. H., Ajayi, O. O., Fenske, G. R., & David, S. (2009): *Effect of friction stir processing on the tribological performance of high carbon steel*, Wear, Vol. 267(1-4), pp. 350–355.

ASM International Handbook Committee. (2007): *ASM Metals Handbook Vol 1 - Properties and Selection: Irons, Steels, and High-Performance Alloy,* ASM International.

ASM International Handbook Committee. (2007): *ASM Metal Handbook Vol 9: Metalography and Microstructures,* ASM International.

Arora, A., Nandan, R., Reynolds, A. P., & Debroy, T. (2009): *Torque , power requirement and stir zone geometry in friction stir welding through modeling and experiments,* Scripta Materialia, Vol. 60(1), pp. 13–16.

Atapour, M., Pilchak, A., Frankel, G. S., & Williams, J. C. (2010). *Corrosion behaviour of investment cast and friction stir processed Ti–6Al–4V*, Corrosion Science, Vol. 52(9), pp. 3062–3069.

Babu, P. D., Balasubramanian, K.R., & Buvanashekaran, G. (2011): *Laser surface hardening: a review*, International Journal of Surface Science and Engineering, Vol. 5, pp. 131–151.

Berbon, P.B., Bingel, W.H., Mishra, R.S., Bampton, C.C., & Mahoney, M.W. (2001): *Friction Stir Processing: A tool to homogenize nanocomposites Aluminum Alloys,* Scripta Material, 44, pp. 61–66.

Callister Jr, W. D. (2001): *Fundamentals of Materials Science and Engineerin,* John Wiley & Sons, Inc.

Chabok, A., & Dehghani, K. (2010): *Formation of nanograin in IF steels by friction stir processing*, Materials Science and Engineering A, Vol. 528(1), pp. 309–313.

Chen, Y. C., & Nakata, K. (2009): *Evaluation of microstructure and mechanical properties in friction stir processed SKD61 tool stee,*. Materials Characterization, Vol. 60(12), pp. 1471–1475.

Çam, G. (2011): *Friction stir welded structural materials: beyond Al-alloys*, International Materials Reviews, Vol. 56(1), pp. 1–48.

Dehghani, K., & Chabok, A. (2011): *Dependence of Zener parameter on the nanograins formed during friction stir processing of interstitial free steels*, Material Science Engeering A, Vol. 528, pp. 4235–4330.

Feng, A. H., & Ma, Z. Y. (2007): *Enhanced mechanical properties of Mg–Al–Zn cast alloy via friction stir processing*, Scripta Materialia, Vol. 56(5), pp. 397–400.

Galvão, I., Loureiro, A., & Rodrigues, D. M. (2012): *Influence of process parameters on*

the mechanical enhancement of copper-DHP by FSP, Vol. 445, pp. 631–636.

Geels, K., Fowler, D. B., Kopp, W.U., & Rükert, M. (2007): *Metallographic and Materialograhic Specimen Preparation, Light Microscopy, Image Analysis and Hardness Testing,* ASTM International.

Giles, T. L., Oh-Ishi, K., Zhilyaev, A. P., Swaminathan, S., Mahoney, M. W., & McNelley, T. R. (2008): *The Effect of Friction Stir Processing on the Microstructure and Mechanical Properties of an Aluminum Lithium Alloy*, Metallurgical and Materials Transactions A, Vol. 40(1), pp. 104–115.

Grewal, H. S., Arora, H. S., Singh, H., & Agrawal, A. (2013): *Surface modification of hydroturbine steel using friction stir processing*, Applied Surface Science, Vol. 268, pp. 547–555.

Khandkar, M.Z.H., Khan, J.A., & Reynolds, A.P. (2003): *Prediction of temperature distribution and thermal history during friction stir welding: input torque based model*, Science and Technology of Welding & Joining, Vol. 8, pp. 165–174

Kulak, G. L., Fisher, J. W., & Struik, J. H. A. (2001): *Guide to Design Criteria for Bolted and Riveted Joints,* American Instituite of Steel Construction.

Kwon, I., Baek, S., & Yu, H. (2003): *The use of electrochemical and mechanical property correlations to monitor the degradation of Cr – Mo – V turbine casing steel*, Vol. 80, pp. 157–165.

Leitão, C., Louro, R., & Rodrigues, D. M. (2012): *Using torque sensitivity analysis in accessing Friction Stir Welding/Processing conditions*, Journal of Materials Processing Technology, Vol. 212(10), pp. 2051–2057.

Ljubljana, U. :*Micro-learning*. Applied Metallurgy: http://www.fgg.uni-lj.si/kmk/esdep/master/wg02/l0100.htm.

Ma, Z.Y., Sharma, S.R., Mishra, R.S., & Mahoney, M.W. (2003): *Microstructural modification of cast aluminum alloys via friction stir processing,* Material Science Forum, Vols. 426–432, pp. 2891–96.

Martin, R. & Evans, D. (2000): *Reducing cost in aircraft: The metals affordability iniciative consortium,* Journal JOM, Vol. 52(3), pp. 24-28.

Mehranfar, M., & Dehghani, K. (2011): *Producing nanostructured super-austenitic steels by friction stir processing*, Materials Science and Engineering A, Vol. 528(9), pp. 3404–3408.

Mishra, R. S., Mahoney, M. W., Mcfadden, S. X., Mara, N. A., & Mukherjee, A. K. (2000): *High strain rate superplasticity in a friction stir processed 7075 Al Alloy*, Scripta Materialia, Vol. 42, pp. 163–168.

Mishra, R.S., Ma, Z.Y., Ma & Charit, I. (2002): *Multi-sheet structures in 7475 aluminum by friction stir welding in concert with post-weld superplastic forming,* Scripta Materialia, Vol. 47, pp. 631-636.

Nah, H., & Kim, K. (2011): *Establishment of Slip Coefficient for Slip Resistant Connection*, David Publishing, Vol. 5(2), pp. 112–120.

Oh-ishi, K., & Mcnelley, T. R. (2004): *Microstructural Modification of As-Cast NiAl Bronze by Friction Stir Processing*, Metallurgical and Materials Transactions A, Vol. 3, pp. 2951–2961.

Oliveira, C. K. N., Benassi, C. L., & Casteletti, L. C. (2006): *Evaluation of hard coatings obtained on AISI D2 steel by thermo-reactive deposition treatment*, Surface and Coatings Technology, Vol. 201(3-4), pp. 1880–1885.

Pan, W., Yu, G., & Huang, J. (1998): *Mechanical properties of ion-plated TiN films on AISI D2 steel*, Surface and Coatings Technology, Vol. 110, pp. 111–119.

Pew, J.W., Nelson, T.W., & Sorensen, C.D. (2007): *Torque based weld power model for friction stir welding*, Science and Technology of Welding & Joining, Vol. 12, 341–347.

Santella, M. L., Engstrom, T., Storjohann, D., & Pan, T.-Y. (2005): *Effects of friction stir processing on mechanical properties of the cast aluminum alloys A319 and A356*, Scripta Materialia, Vol. 53(2), pp. 201–206.

Spowart, J.E., Ma, Z.Y., & Mishra, R.S. (2003): *Friction Stir Welding and Processing II*, Jata, K.V., Mahoney, M.W, Mishra, R.S., Semiatin, S.L, and Lienert, T., eds., TMS, Warrendale, PA pp. 243–52.

Su, J.-Q., Nelson, T. W., & Sterling, C. J. (2005): *Friction stir processing of large-area bulk UFG aluminum alloys*, Scripta Materialia, Vol. 52(2), pp. 135–140.

Xing-hao, D. U., & Bao-lin, W. U. (2008): *Using friction stir processing to produce ultrafine-grained microstructure in AZ61 magnesium alloy*, Transactions of Nonferrous Metals Society of China, Vol. 18, 562–565.

Yadav, D., & Bauri, R. (2012): *Effect of friction stir processing on microstructure and mechanical properties of aluminium*, Materials Science and Engineering A, Vol. 539, pp. 85–92.

Yoon, S. Y., Yoon, S.-Y., Chung, W.-S., & Kim, K. H. (2004): *Impact-wear behaviors of TiN and Ti–Al–N coatings on AISI D2 steel and WC–Co substrates*, Surface and Coatings Technology, Vol. 177-178, pp. 645–650.

[This page intentionally left blank]

[This page intentionally left blank]

ANNEX A

There are several classification systems in which the steels are categorized according to the applications, mechanical properties or fabrication method. In current work the substrate materials are classified according to the European Standards 10025–10027, which uses a nomenclature as follows to identify the steels: S 355 J2+ Z35+ M. In this nomenclature S represents the Steel Group (see Table A.1), 355 correspond to the minimum yield strength, J2 represents the notch toughness category (see Table A.1) and Z35 and M identify special requirements and treatment conditions, respectively.

Table A.1 Legend of the EN 10025

<table>
<tr><td colspan="2" rowspan="2">Steel Group</td><td>Mecanical Propreties (2)</td><td>Mecanical Propreties (3)</td></tr>
<tr><td></td><td rowspan="10">JR: Indicates that the Charpy Impact test was conducted to 27 Joules minimum at room temperature

J0: Indicates that the Charpy Impact test was conducted to 27 Joules minimum at 0ºC

J2: Indicates that the Charpy Impact test was conducted to 27 Joules minimum at -20ºC

K2: Indicates that the Charpy Impact test was conducted to 40 Joules minimum at -20ºC

G3: Indicates delivery conditions are at manufacturer's discretion</td></tr>
<tr><td rowspan="11">Specifications</td><td>G: Steel casting</td><td></td></tr>
<tr><td>S: Structural Steel</td><td rowspan="4">Minimum yield strength for smallest thickness</td></tr>
<tr><td>P: Pressure Vessel Steels</td></tr>
<tr><td>L: Line pipe Steels</td></tr>
<tr><td>E: Engineering Steels</td></tr>
<tr><td>B: Steels for Reinforcing Concrete</td><td>Characteristic yield strength</td></tr>
<tr><td>Y: Steels for Prestressing Concrete</td><td rowspan="2">Minimum tensile strength</td></tr>
<tr><td>R: Steels for on in the form of Rails</td></tr>
<tr><td>H: Steels for Cold Rolled Flat Products of high Strength Steels for cold forming</td><td rowspan="2">Characteristic yield strength</td></tr>
<tr><td>D: Flat Products for Cold Forming (except H); DC for Cold Rolled products; DD for Hot Rolled products and DX for Non specified rolled condition</td></tr>
</table>

[This page intentionally left blank]

[This page intentionally left blank]